ROYAL SOCIETY OPEN SCIENCE

Adsorption and corrosion inhibition behavior of new theophylline-triazole based derivatives for steel in acidic medium

Journal:	*Royal Society Open Science*
Manuscript ID	RSOS-181738.R1
Article Type:	Research
Date Submitted by the Author:	14-Jan-2019
Complete List of Authors:	Espinoza Vazquez, Araceli ; Universidad Nacional Autonoma de Mexico Facultad de Quimica Rodríguez Gómez, Francisco Javier; Universidad Nacional Autonoma de Mexico Facultad de Quimica Martínez Cruz, Ivonne Karina; Universidad Autonoma Metropolitana Azcapotzalco Ángeles Beltrán, Deyanira; Universidad Autonoma Metropolitana Azcapotzalco Negrón Silva, Guillermo Enrique; Universidad Autonoma Metropolitana Azcapotzalco Palomar Pardavé, Manuel; Universidad Autonoma Metropolitana Azcapotzalco Lomas Romero, Leticia; Universidad Autonoma Metropolitana Iztapalapa Pérez Martínez, Diego; Universidad Autonoma Metropolitana Iztapalapa Navarrete López, Alejandra M. ; Universidad Autónoma Metropolitana-Azcapotzalco, Ciencias Básicas
Subject:	Synthetic chemistry < CHEMISTRY
Keywords:	Theophylline, corrosion inhibition, API 5L X52 steel, quantum chemical calculation, acid
Subject Category:	Chemistry

January 11, 2019

Andrew Harned
Associate Editor, Royal Society Open Science
Texas Tech University

It is a pleasure to send the corrected version of the manuscript ID: *RSOS-181738*

Adsorption and corrosion inhibition behavior of new theophylline-triazole based derivatives for steel in acidic medium

Authors:

Araceli Espinoza-Vázquez[a], Francisco Javier Rodríguez-Gómez[a], Ivonne Karina Martínez-Cruz[b], Deyanira Ángeles-Beltrán,[b] Guillermo E. Negrón-Silva[b*], Manuel Palomar-Pardavé,[c] Leticia Lomas Romero,[c] Diego Pérez-Martínez[c], Alejandra M. Navarrete-López[b]

We have answered all comments and suggestions from the referees. We would be grateful for the attention given to our letter and accompanying manuscript and be happy to provide any further information as deemed necessary.

With our best regards,

Dr. Guillermo E. Negrón Silva
Profesor-Investigador
Laboratorio de Química de Materiales
Departamento de Ciencias Básicas
División de Ciencias Básicas e Ingeniería
Laboratorios G-112
Tel.: 53189593

Reviewer comments to Author:
Reviewer: 1

Comments to the Author(s)
Comments on RSOS-181738
Title: Adsorption behavior of new theophylline-triazole based derivatives as effective corrosion inhibitors for steel in acidic medium
Series of theophylline derivatives containing 1,2,3-triazole moieties were synthesized, characterized, and studied as corrosion inhibitor for API 5L X52 steel in 1 M HCl medium by Espinoza-Vázquez et al. Electrochemical techniques namely EIS and PDP were used in the investigation and was supported with SEM and EDS analysis. The study is of interest and the results presented well interpreted. However, MINOR revision needs to be done before publication. Here are some of the issues:

1. *Individual graph in the PDP plot should be labeled since authors are using line plotting. Otherwise, they should replot with line and symbol*

Reply: We agree with these comments; thus, we have modified Figure 3 as follows:

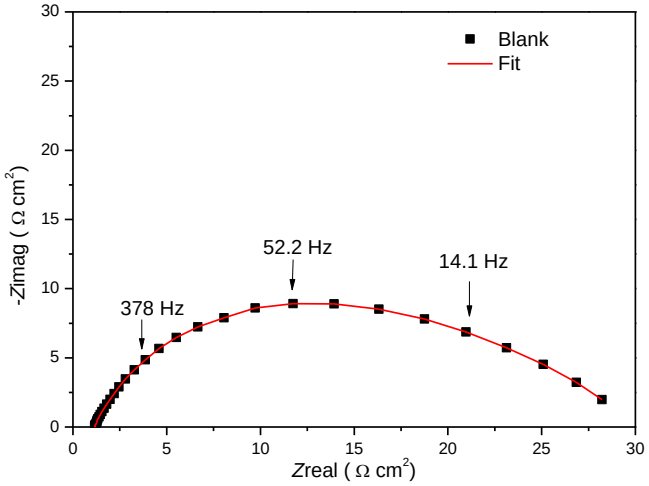

2. *The mechanism of adsorption of the studied inhibitor should be fully discussed.*

Reply: We agree with these comments, therefore, in the revised version we have added the following section regarding this comment:

Adsorption mechanism

The corrosion inhibition of API 5L X52 in HCl 1M provoked by 1,2,3-triazoles 1,4-disubstited molecules can be explained as follows (Figure 9): The protonated species of the organic compounds interact, throughout Columbic forces, with previously adsorbed chlorides ions (Cl-) present on the API 5L X52 steel surface which results in physisorption of the inhibitor molecules. This way, the inhibitor molecules compete with H^+ for electrons on steel surfaces [67]. Moreover, the donation of lone electrons pairs of nitrogen atoms to the empty orbital of Fe atoms would induce a chemisorption process of the organic molecule [68] and the accumulation of negative charges on the steel surface can be transferred from the d orbital of Fe to unoccupied $\pi*$ (anti-bonding) of 1,2,3-triazoles 1,4-disubstited molecules (retro-donation) [69], see Figure 9a and 9b. The combination of these two types of adsorption mechanisms is carried out for the compounds evaluated. However, the compound 7 (Figure 9b) showed a stronger interaction

(chemisorption) by nitrogen heteroatoms that have free electron pairs with steel, demonstrated with thermodynamic analysis using the Langmuir model.

67. Hamania H, Douadia T, Daouda D, Al-Noaimic M, Rikkouha R, Chafaa S. 2017. 1-(4-Nitrophenylo-imino)-1-(phenylhydrazono)-propan-2-one as corrosion inhibitor for mild steel in 1 M HCl solution: Weight loss, electrochemical, thermodynamic and quantum chemical studies, J. Electroanalyt. Chem. 801,425–438.
68. Singh P, Quraishi MA. 2016. Corrosion inhibition of mild steel using Novel Bis Schiff's Bases as corrosion inhibitors: Electrochemical and Surface. Measurement 86, 114–124.
69. Haldhar R, Prasad D, Saxena A. 2018. Myristica fragrans extract as an eco-friendly corrosion inhibitor for mild steel in 0.5 M H2SO4 solution, J. Environm. Chem. Eng. 6, 2290–2301

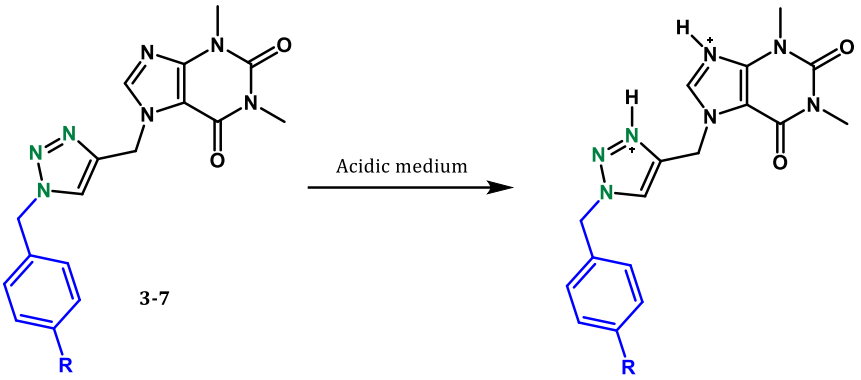

Compound	R
3	-H
4	-F
5	-Cl
6	-Br
7	-I

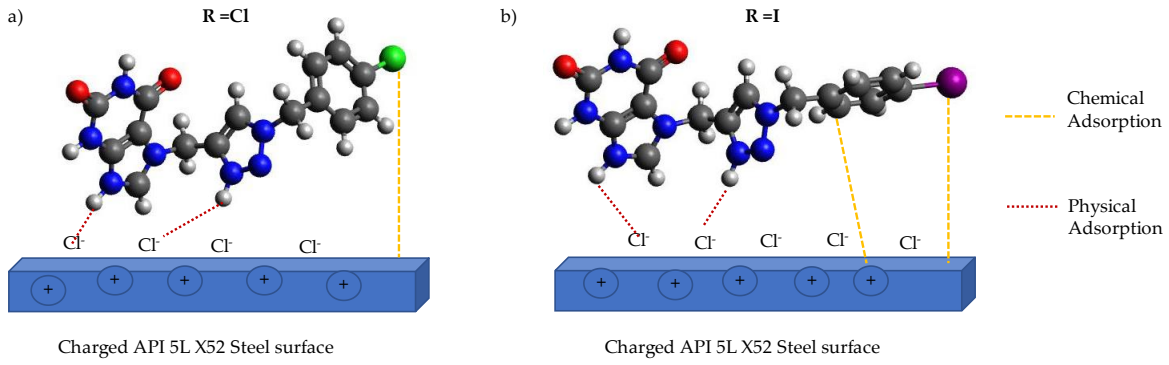

Figure 9. Schematic representation of the adsorption behavior of inhibitor on API 5L X52 steel surface immersed in 1M HCl.

70. *The authors should present the OCP-time graph to convince readers that OCP stability was achieved before measurements.*

Reply: We agree with this comment therefore in the revised version we have included the following:

… Fig. 3a shows the variations in time of the open circuit potential (OCP) in static conditions at 50 ppm, at the electrode made of API 5L X52 steel in presence of different inhibitor concentrations. It should be mentioned that it was necessary the stabilization of the OCP previously to do the EIS determinations. The steady state was reached after 1700 seconds…

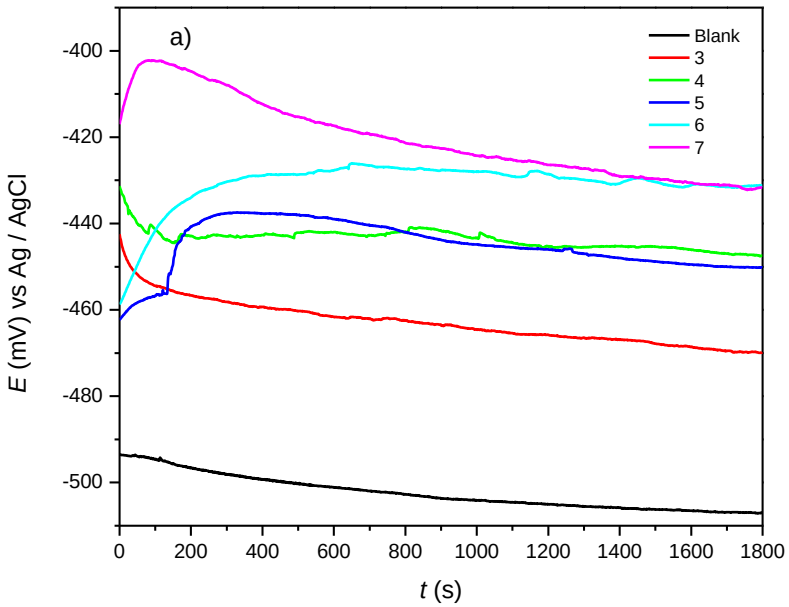

Figure 3 a) Open Circuit Potential (OCP) vs time of theophylline-triazoles derivatives at 50 ppm

71. *Additional surface analysis like AFM, XRD, and/or XPS is needed. This will greatly improve the quality of this manuscript.*

Reply: The reviewer is right, however, at this moment we do not have the equipment nor the resources to perform the requested surfaces analysis. Notwithstanding, we believe that the experimental results showed in the SEM-EDS section are sufficient to directly relate them to the anticorrosive capacity of the inhibitors reported in this work.

Reviewer: 2

Comments to the Author(s)

The authors have studied five new Theophylline derivatives bearing Triazole moieties for their corrosion inhibition behavior on steel in 1M HCl solution. All the synthesized inhibitors have been very well characterized through their spectral data. The paper can be considered for publication after satisfactory response to following comments:

1. *How did the authors convert Molar solution to ppm concentration?*

Reply: There was an initial concentrated solution in order to make dilutions and finally, diluted solutions were obtained by sampling different aliquots completing with DMF However, inhibitor concentrations are usually reported as ppm (part per million, mg/kg or mg/liter).

Did the authors check the inhibiting effect of DMF alone and in the presence of inhibitor because DMF also acts as inhibitor?

Reply: In this case, the compounds have solubility in DMF, so it was used as a solvent, however, it was found that, at the evaluated working conditions, DMF corrosion inhibitor capacity is practically null.

2. *In EDX Fig, the presence of inhibitor is not visible. How did authors confirm the adsorption of inhibitor on steel surface?*

Reply: As can be noted from Figure 10 in the revised version the peak associated with carbon is much intense in the presence of the inhibitor, see Figures 10f and 10h that on the bare steel sample, see Figure 10b therefore, this may be indicated of the presence of the inhibitors on the steel sample surface. In the revised version, we have added the following to clarify this point.

…are not observed in the chemical analysis (Figures 10f and 10h). However, as can be noted from Figure 10 in the revised version the peak associated with carbon is much intense in the presence of the inhibitor, see Figures 10f and 10h that on the bare steel sample, see Figure 10b therefore, this may be indicated of the presence of the inhibitors on the steel sample surface.

3. *There is no explanation of βa and βc values in Tafel polarization study. The sign of βc should be negative.*

Reply: We agree with this observation, thus in the revised version we have modified Table 2 as follows:

Table 2. Electrochemical parameters obtained by means of polarization curves for 1,2,3-triazoles 1,4-disubstited in API 5L X52 steel immerse in HCl 1M

Inhibitor	C (ppm)	E_{corr} (mV) vs Ag/AgCl	bc (mV dec^{-1})	ba (mV dec^{-1})	i_{corr} (mA/cm^2)	η_{pol} (%)
Blank	0	-421.2	-106.5	84.6	0.32	-
3	5	-450.8	-107.0	54.3	0.04	87.3
3	50	-470.1	-109.5	75.0	0.04	86.9
4	5	-448.0	-163.4	80.4	0.08	76.6
4	50	-439.9	-158.8	74.7	0.04	87.0
5	5	-447.6	-146.8	52.6	0.07	79.4
5	50	-441.0	-110.2	66.3	0.02	71.0
6	5	-413.4	-122.1	30.5	0.02	94.3
6	50	-427.2	-136.2	48.4	0.02	93.5
7	5	-410.8	-161.2	52.1	0.03	90.3
7	50	-425.3	-132.2	69.5	0.04	88.2

4. *The range for polarization ± 500 mV is very high. Is there any reason for this? The sweep rate should be 0.1mV /sec.*

Reply: About the sweep rate, in literature it is recommended to use 0.1 to 1 mV s-1, as a good practice.

5. *In EIS study, Bode plot should be provided to understand the adsorption behavior of inhibitors.*

Reply: We agree with this observation. Therefore, in the revised version we have included the bode plots.

…The Bode plots for API 5L X52 steel in the absence and presence of various concentrations of 1,2,3-triazoles 1,4-disubstited are represented in Fig. 5. An ideal capacitor is characterized by a fixed value of slope (unity) and phase angle (−90°). The increase in the values of phase angle in presence of different inhibitor concentrations suggest that surface roughness of API 5L X52 steel decreased due to formation of protective film by theophylline-triazole derivative [44]. The result indicated that there was two-time constant coupled, and the system could be described by three resistances which consists of electrolyte resistance (R_s), charge transfer resistance (R_{ct}), organic molecules adsorbed resistance (R_{mol}) and double layer capacitance, as shown in Fig 2b. While, in absence inhibitor the phase angle vs log frequency shows one-time constant attributed to charge transfer resistance [45].
Finally, the corrosion inhibition effectiveness of 1,2,3-triazoles 1,4-disubstited can also be interpreted in the real impedance values axis of the Bode modulus plots which also increases as the concentration increase (Fig. 5 a, c, e, g and h)…

[44] Ebenso EE, Kabanda MM. 2012. Electrochemical and quantum chemical investigation of some azine and thiazine dyes as potential corrosion inhibitors for mild steel in hydrochloric acid solution. Ind. Eng. Chem. Res. 51, 12940–12958. *Ind. Eng. Chem. Res.* 51, 12940–12958.
[45] Zhang H, Pang X, Zhou M, Liu C, Wei L, Gao K. 2015. The behavior of pre-corrosion effect on the performance of imidazoline-based inhibitor in 3 wt.% NaCl solution saturated with CO_2, *Appl. Surf. Sci.* 356: 63–72.

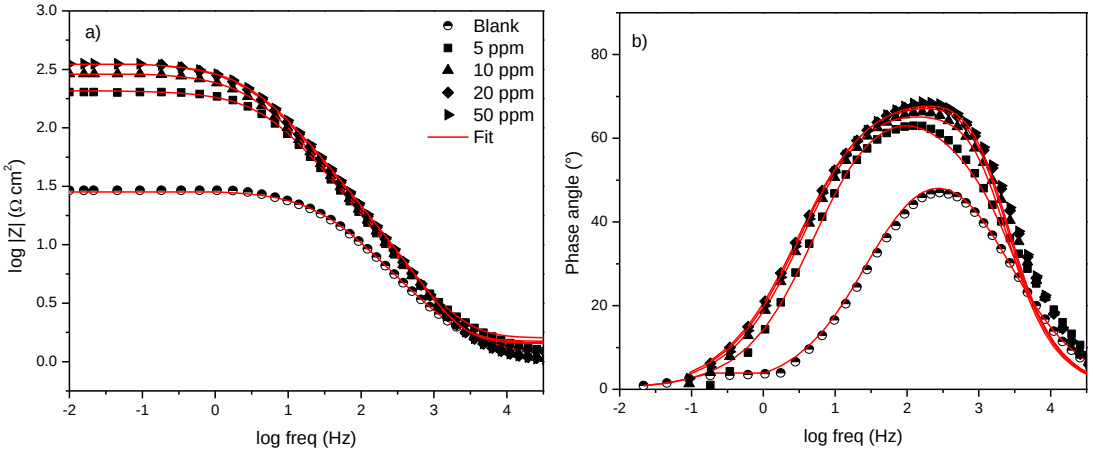

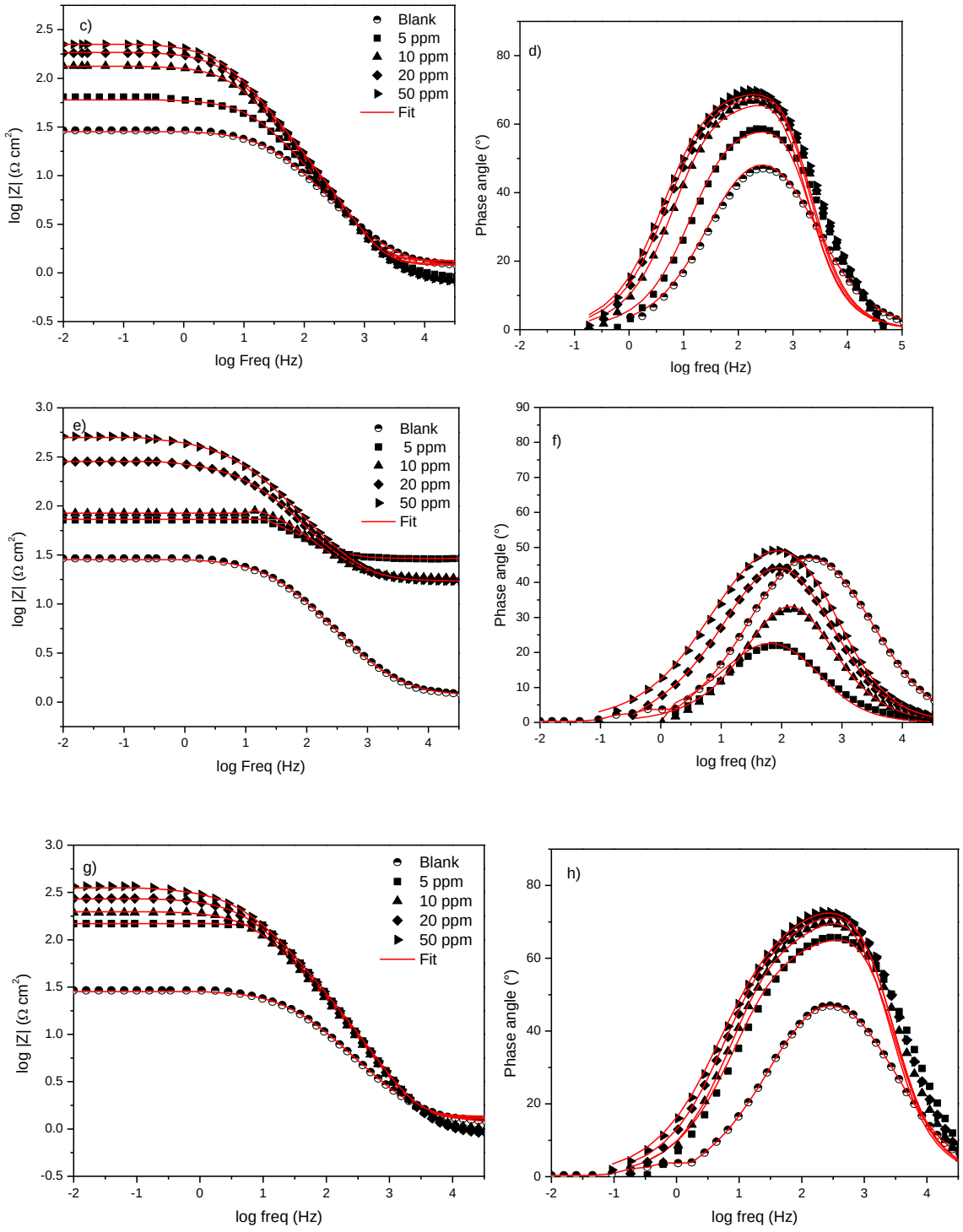
c)
Blank
5 ppm
10 ppm
20 ppm
50 ppm
Fit
log |Z| (Ω cm²)
log Freq (Hz)
d)
Phase angle (°)
log freq (Hz)
e)
Blank
5 ppm
10 ppm
20 ppm
50 ppm
Fit
log |Z| (Ω cm²)
log Freq (Hz)
f)
Phase angle (°)
log freq (hz)
g)
Blank
5 ppm
10 ppm
20 ppm
50 ppm
Fit
log |Z| (Ω cm²)
log freq (Hz)
h)
Phase angle (°)
log freq (Hz)

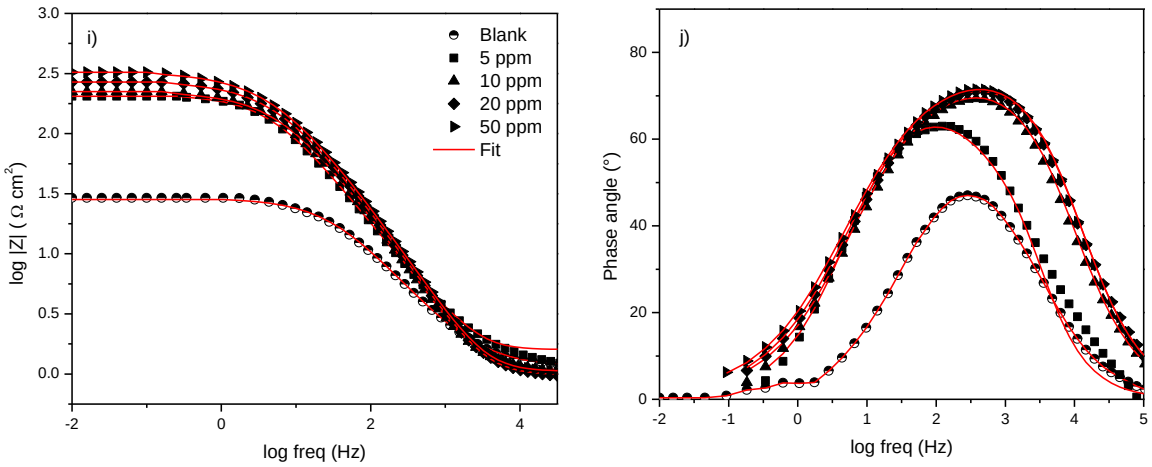

Figure 5 Bode diagrams of theophylline-triazoles compounds: a) 3, b) 4, c) 5, d) 6 and e) 7 immersed API 5L X52 steel at different inhibitor concentrations.

6. *What is r mol? Is it film resistance? Clarify*

Reply: The Rmol term refers to the "resistance of the organic molecules adsorbed" usually employed for different authors in papers related with inhibitors. Even when some authors name this value as "film resistance", we prefer not to use this term since there could be confusion with the formation of an organic film coming from the molecules, instead of an interface formed by adsorbed molecules to the metallic surface.

7. *The mechanism of inhibition should be clearly discussed. Which form of the inhibitor is predominantly adsorbed: Neutral or protonated? It should be clearly stated based on DFT calculation.*

Reply: We agree with this comment thus, in the revised version of our manuscript we have included a new section regarding the mechanism of inhibition

Adsorption mechanism

The corrosion inhibition of API 5L X52 in HCl 1M provoked by 1,2,3-triazoles 1,4-disubstited molecules can be explained as follows (Figure 9): The protonated species of the organic compounds interact, throughout Columbic forces, with previously adsorbed chlorides ions (Cl-) present on the API 5L X52 steel surface which results in physisorption of the inhibitor molecules. This way, the inhibitor molecules compete with H^+ for electrons on steel surfaces [67]. Moreover, the donation of lone electrons pairs of nitrogen atoms to the empty orbital of Fe atoms would induce a chemisorption process of the organic molecule [68] and the accumulation of negative charges on the steel surface can be transferred from the d orbital of Fe to unoccupied $\pi*$ (anti-bonding) of 1,2,3-triazoles 1,4-disubstited molecules (retro-donation) [69], see Figure 9a and 9b. The combination of these two types of adsorption mechanisms is carried out for the compounds evaluated. However, the compound 7 (Figure 9b) showed a stronger interaction (chemisorption) by nitrogen heteroatoms that have free electron pairs with steel, demonstrated with thermodynamic analysis using the Langmuir model.

67. Hamania H, Douadia T, Daouda D, Al-Noaimic M, Rikkouha R, Chafaa S. 2017. 1-(4-Nitrophenylo-imino)-1-(phenylhydrazono)-propan-2-one as corrosion inhibitor for mild steel in 1 M HCl solution: Weight loss, electrochemical, thermodynamic and quantum chemical studies, J. Electroanalyt. Chem. 801,425–438.
68. Singh P, Quraishi MA. 2016. Corrosion inhibition of mild steel using Novel Bis Schiff's Bases as corrosion inhibitors: Electrochemical and Surface. Measurement 86, 114–124.
69. Haldhar R, Prasad D, Saxena A. 2018. Myristica fragrans extract as an eco-friendly corrosion inhibitor for mild steel in 0.5 M H2SO4 solution, J. Environm. Chem. Eng. 6, 2290–2301

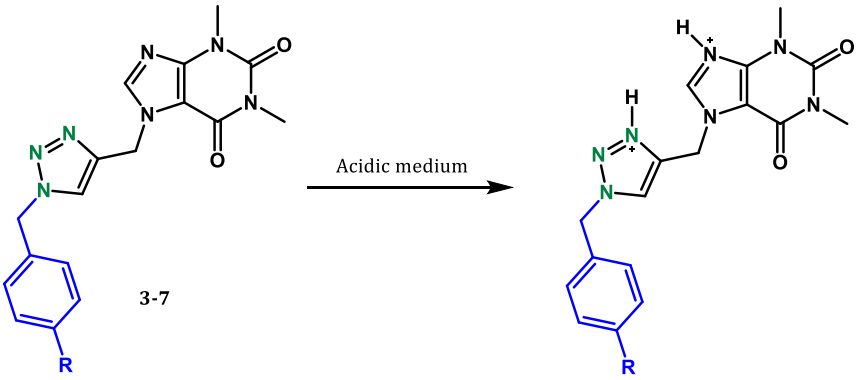

Compound	R
3	-H
4	-F
5	-Cl
6	-Br
7	-I

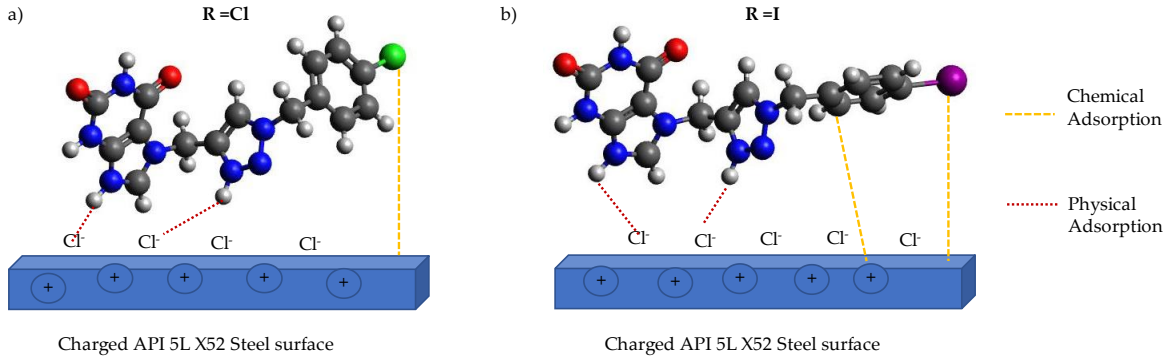

Figure 9. Schematic representation of the adsorption behavior of inhibitor on API 5L X52 steel surface immersed in 1M HCl.

Quantum chemical calculations have also been included within a new section named "*Theoretical assessment*". Alejandra M. Navarrete-López was responsible for the calculations.

4.1 Theoretical assessment

The presence of nitrogen as heteroatom in the inhibitor molecules provides high tendency toward protonation in aqueous acidic medium. Under these conditions the calculations were carry out for the complete set of electrons and the geometry of involved structures was fully optimized. In other words, the nitrogen atoms hold positive charge by

adding of hydrogen atoms and the solvent (water) effect is including with the Solvation Model based on Density (SMD) [33]. The results of the geometry optimization of the selected compounds in acidic medium and solvent effect are presented in Figure 11.

A very important fact in the adsorption over the metallic surface is the planar configuration of the inhibitor molecules. The frameworks of these geometries show no planar configurations for all the inhibitors. Some angles are showed in Figure 11, the halogen substitute has an important effect over the dihedral angle, particularly with Iodine.

Quantum-chemical indexes EHOMO, ELUMO, GAP, hardness η, and dipole moment are summarized in Table 4. It is known that EHOMO is often related to electron donation ability of the inhibitor molecules toward the metallic surface atoms, and it is expected that a higher EHOMO value would favor a greater charge transfer [70]. According to these results, the values of EHOMO show the following behavior: compound 7 > compound 6 > compound 5 > compound 3 > compound 4. In this case, the notorious largest EHOMO corresponds to compound 7 in line with the aforementioned experiments at low concentrations and the lowest EHOMO corresponds to compound 4 that in terms of activity is the worst inhibitor.

Some other authors (for instance [71]) have found that a smaller value of the hardness is related to greater stability of the surface-inhibitor complex formed. The trend that we got was 4 > 3 > 5 > 6 > 7, as it can be observed in Table 4. Then the complex metallic surface-compound 7 presents the best stability and inhibition efficiency at low concentrations.

Moreover, smaller values of ELUMO present better capacity of the inhibitor to accept electrons, for this property the trend with solvent was compound 7 < 4 < 5, 6 < 3. Negative values of ELUMO indicate the capability to accept electrons too. Nevertheless, there is not a clear relationship between the above last two properties.

For the overall electrophilicity and according to the computed values (see Table 5), compound 7 exhibited a better nucleophilic character with solvent effect. Whereas compound 4 was lower than the rest. Therefore, a better interaction of compound 7 with the metallic surface would be expected than for the rest of compounds, the differences are not significant.

The Hirshfeld atomic charges for the most important centers with solvent effect are summarized in Table 6. Redistribution of the charge is observed by the presence of the substituent, the atoms that have a larger negative charge, suggests that those are active centers with excess charges that it could act as a nucleophilic group. The most favorable sites for the interaction with the metal surface are the Oxygen atoms, 24 and 25, see Figure 11 and Table 6, for all the selected compounds. As it has been expected, fluorine in compound 4 is the best electro-attractor followed by Chlorine, the halogen substitutes are active sites for the inhibition. The Carbon 8, in all the compounds, is another nucleophilic center. The Carbon 13 in compound 7 also gains charge.

Experimental data revels that compound 7 is the best inhibitor of the corrosion, the geometric structure and the parameters here studied such as EHOMO, hardness, electrophilicity and atomic charges support this fact.

Table 6. *Atomic Hirshfeld charges for the different inhibitor compounds. See the Figure 11 for the atomic labels.*

Number	Atom	Compound 3	Compound 4	Compound 5	Compound 6	Compound 7
1	N	-0.011	-0.005	-0.007	-0.011	-0.003
2	N	0.305	0.306	0.306	0.310	0.313
3	N	0.087	0.088	0.087	0.087	0.090
4	C	0.164	0.178	0.177	0.151	0.188
5	C	0.074	0.075	0.074	0.075	0.077
6	C	0.275	0.275	0.276	0.274	0.276
7	C	0.210	0.218	0.219	0.216	0.227

8	C	-0.020	-0.019	-0.015	-0.012	-0.013
9	C	0.020	0.040	0.041	0.044	0.036
10	C	0.027	0.048	0.048	0.050	0.001
11	C	0.015	0.026	0.024	0.013	0.029
12	C	0.015	0.026	0.023	0.012	0.027
13	C	0.017	0.094	0.036	-0.004	-0.031
14	**H**	**0.000**	**-0.167**	**-0.110**	**-0.038**	**-0.038**
15	N	0.025	0.024	0.025	0.025	0.025
16	C	0.358	0.358	0.359	0.356	0.358
17	N	0.245	0.245	0.245	0.245	0.245
18	C	0.165	0.165	0.165	0.165	0.166
19	C	0.015	0.015	0.014	0.015	0.015
20	N	0.165	0.165	0.165	0.165	0.165
21	C	0.213	0.213	0.212	0.215	0.213
22	N	0.127	0.127	0.127	0.127	0.127
23	C	0.271	0.271	0.271	0.270	0.271
24	O	-0.353	-0.354	-0.352	-0.343	-0.352
25	O	-0.411	-0.411	-0.410	-0.411	-0.411

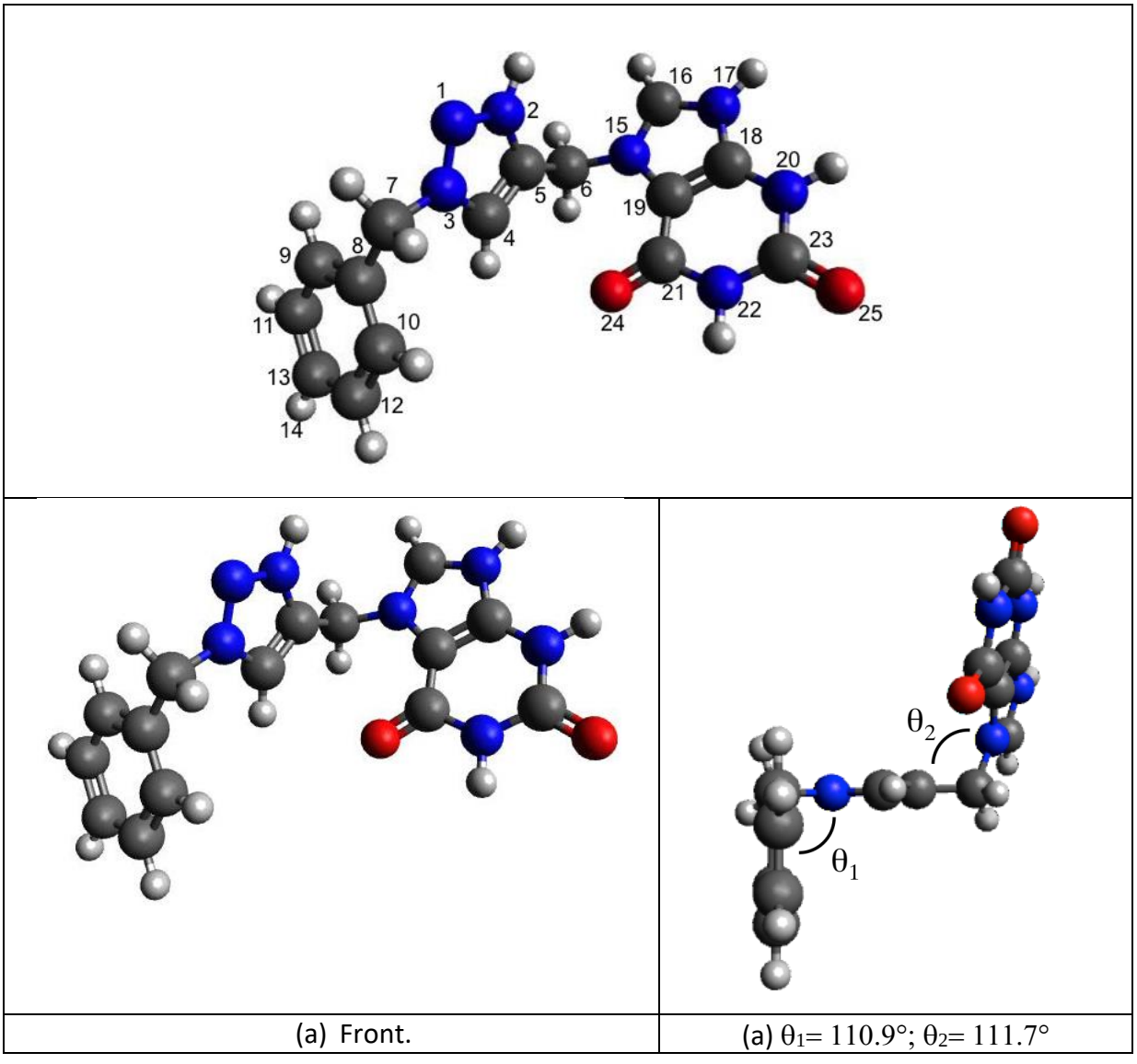

(a) Front. (a) θ_1= 110.9°; θ_2= 111.7°

Dihedral = 100.6°	
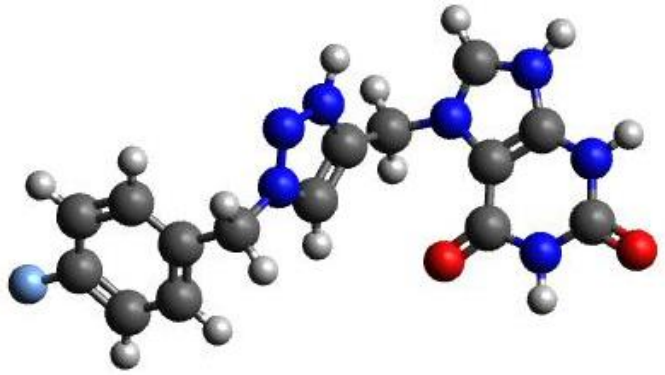	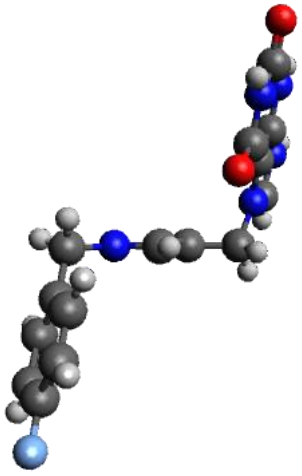
(b) Front, F= blue Dihedral = 97.3°	(b) θ_1= 111.1° ; θ_2= 111.0°
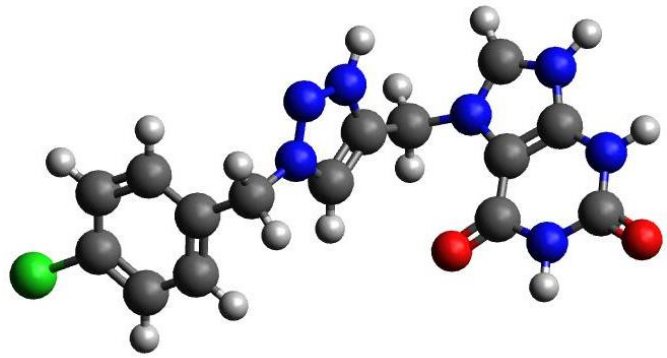	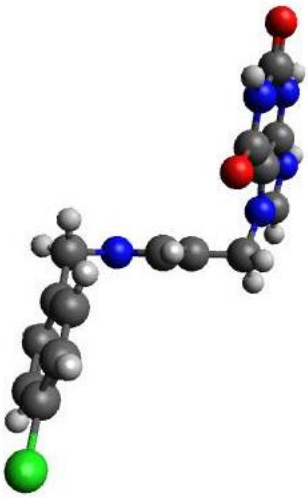
(c) Front, Cl= Green Dihedral = 96.4°	(c) θ_1= 111.1° ; θ_2= 111.2°
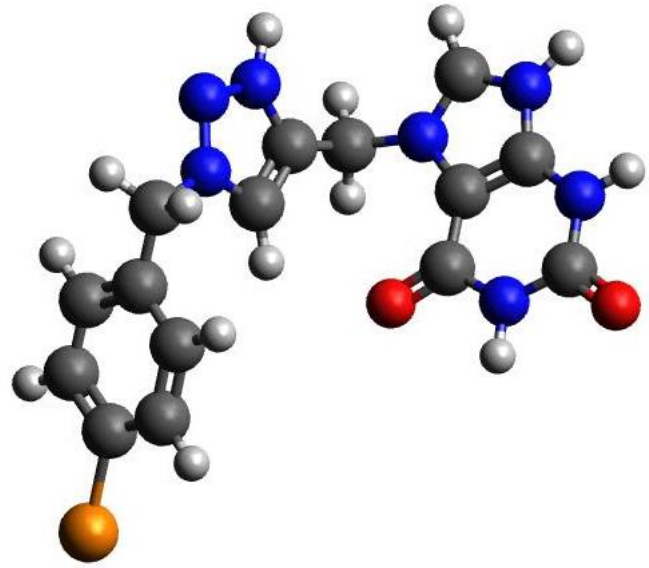	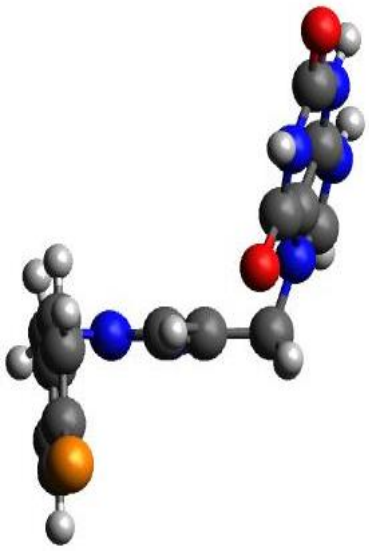
(d) Front, Br= orange	(d) θ_1= 110.7°; θ_2= 111.6°

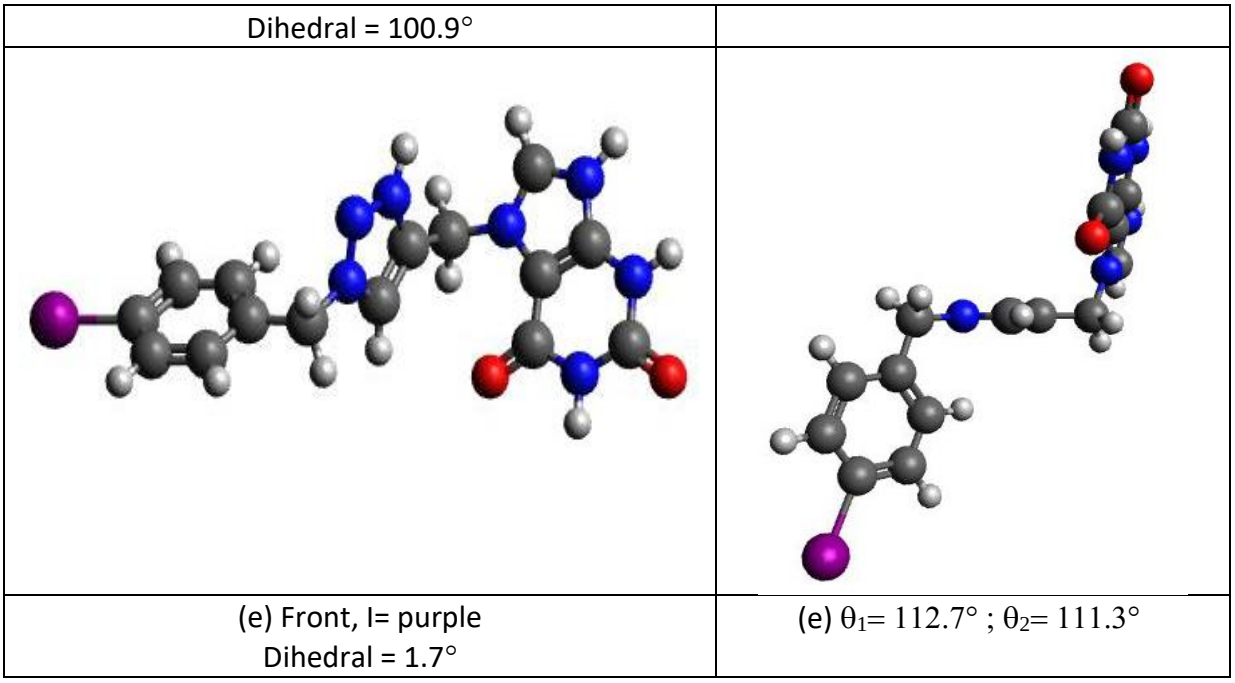

Figure 11. Optimized molecular structures: (a) compound 3, (b) compound 4, (c) compound 5, (d) compound 6, (e) compound 7. Carbon atoms are represented in gray ball, Nitrogen in dark blue, Oxygen in red and Hydrogen in white color. Dihedral angle among 3,7,8 and 10 atoms.

33. Frisch MJ, Trucks GW, Schlegel HB, Scuseria GE, Robb MA, Cheeseman JR, Scalmani G, Barone V, Mennucci B, Petersson GA, Nakatsuji H, Caricato M, Li X, Hratchian HP, Izmaylov AF, Bloino J, Zheng G, Sonnenberg JL, Hada M, Ehara M, Toyota K, Fukuda R, Hasegawa J, Ishida M, Nakajima T, Honda Y, Kitao O, Nakai H, Vreven T, Montgomery JrJA, Peralta JE, Ogliaro F, Bearpark M, Heyd JJ, Brothers E, Kudin KN, Staroverov VN, Kobayashi R, Normand J, Raghavachari K, Rendell A, Burant JC, Iyengar SS, Tomasi J, Cossi M, Rega N, Millam JM, Klene M, Knox JE, Cross JB, Bakken V, Adamo C, Jaramillo J, Gomperts R, Stratmann RE, Yazyev O, Austin AJ, Cammi R, Pomelli C, Ochterski JW, Martin RL, Morokuma K, Zakrzewski VG, Voth GA, Salvador P, Dannenberg JJ, Dapprich S, Daniels AD, Farkas Ö, Foresman JB, Ortiz JV, Cioslowski J, Fox DJ. 2009. Gaussian 09 (Gaussian, Inc., Wallingford CT).
70. Khaled KF. 2008. Molecular simulation, quantum chemical calculations and electrochemical studies for inhibition of mild Steel by triazoles. Electrochim. Acta, 53, 3484-3492.
71. Sahin M, Gece G, Kaerci F, Bligic S. Experimental and theoretical study of the effect of some heterocyclic compounds on the corrosión of low carbon steel in 3.5% NaCl medium. J. Appl. Electrochem., 38, 809-815.

8. Adsorption isotherm should be redrawn by selecting proper values on X and Y axis

Reply: We agree with this suggestion thus, we have recalculated and converted the value on X and Y to millimolar as follows:

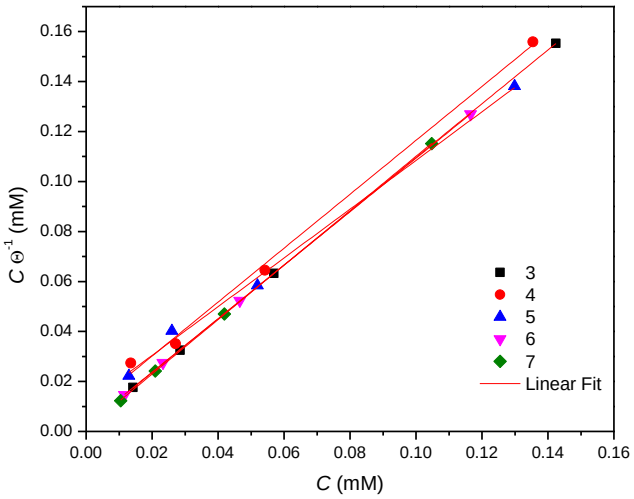

9. *Fig 8: EDX is reported for 5 and 20 ppm concentration while optimum concentration is 50 ppm. Is there any reason for using lower concentration?*

Reply: In this case, we wanted to compare compounds 5 and 7 by using the same concentration (20 ppm) because they had practically the same efficiency value. Actually, we did not compare with 5 ppm.

10. What is the significance of using API5LX52 and 1M HCl?

Reply: API 5L X52 steel was used because it is a metal that is used in the oil industry, while HCl was studied due to its aggressive behavior, even more severe than the usual conditions in plant.

Reviewer: 3

Comments to the Author(s)
COMMENTS ON MANUSCRIPT RSOS-181738
TITLE: Adsorption behavior of new theophylline-triazole based derivatives as effective corrosion inhibitors for steel in acidic medium

COMMENTS
The manuscript reports on the synthesis, characterization of theophylline-triazole based derivatives and evaluation of corrosion inhibition performance for API 5L X52 steel corrosion in 1 M HCl solution. The corrosion inhibition effect was investigated using electrochemical impedance spectroscopy and potentiodynamic polarization techniques complemented by surface morphological characterization of the corroded carbon steel samples without and with the inhibitors with SEM/EDS. The manuscript is of interest in the fields of materials and corrosion. The synthesis and characterization of the compounds used as inhibitors is well treated but the same cannot be said of the corrosion inhibition behavior of the synthesized compounds. In its present form, the manuscript is not recommended for publication in Royal Society Open Science. Major revision of the paper is needed before consideration for publication. The issues to be addressed by the authors are appended below:

(1)The Title of the manuscript should be modified to read "Adsorption and corrosion inhibition behavior of new theophylline-triazole based derivatives for steel in acidic medium"

Reply: We agree with this suggestion therefore we have modified the title as follows:

Adsorption and corrosion inhibition behavior of new theophylline-triazole based derivatives for steel in acidic medium

(2) There are important keywords not listed and the irrelevant ones are listed. Words like Acid, Theophylline, Corrosion inhibition, Steel should form part of the keywords if required by the journal.

Reply: We agree with this observation. In final version, we changed the Keywords as follows:

Keywords: Teophylline, corrosion inhibition, API 5L X52 steel, acid

(3) On page 2 line 14, 'adsorpted' should be corrected to 'adsorbed'. Also in line 24, 'absord' should be corrected to 'adsorb'

Reply: These mistakes have been corrected in the revised version.

... It has been found that molecules with lone electron pairs and/or π-electrons in their structure shows great affinity to be adsorbed into the metallic material [9-12]…

…Several reports have highlighted the capabilities of these compounds to strongly adsorb on metal surfaces, achieving an adequate corrosion inhibition efficiency at low concentrations [25-32]…

(4) The idea that the synthesized compounds were tested as 'environmentally friendly' is rather speculative and not based on experimental evidence as they were not tested experimentally to ensure that they meet the three criteria of a compound to be designated as 'environmentally friendly' which are toxicity, biodegradability and bioaccumulation. Hence the statement in line 31 of page 2 should be revised to clear this ambiguity.

Reply: We agree with this observation; therefore, we have eliminated the ambiguity and speculation by removing the 'environmentally friendly' label from the manuscript.

…These novel compounds were tested as corrosion inhibition species in order to establish structure-activity relationships and to gain further insight into their adsorption properties and the steel protection…

(5) It is not clear if the authors had check the purity of the synthesized compounds given that the melting point range is large as could be seen as follows: Compound 2 (220-226 ^{o}C); Compound 3 (169-172 ^{o}C), Compound 4 (182-186 ^{o}C); Compound 6 (194-198 °C.) Compound 7 (180-184 °C.).

Reply: We have revised and corrected the melting points of all the compounds.

1.1.1. ***...****1,3-dimethyl-7-(prop-2-in-1-yl)-3,7-dihydro-1H-purine-2,6-dione (****2****).*

Compound 2 was synthesized following the procedure described by Ruddarraju et al [21]. A mixture of theophylline (1) (1.98 g, 11 mmol) and potassium carbonate (1.990 g, 14.4 mmol) in DMF (30 mL) were stirred vigorously at room temperature for 20 minutes. After this time, propargyl bromide (1.68 mL, 22.2 mmol) was added and temperature

was increased at 85 °C with vigorous stirring for another 2 h. Then, the mixture was poured in cold water. The compound was recovered as a white powder: yield 80%, m.p. 220-222 °C. ^{1}H NMR (500.13 MHz, $CDCl_3$): δ (ppm)= 2.60 (1H, t, J=2.61 Hz, H12), 3.41 (3H, s, N1-CH_3), 3.60 (3H, s, N3-CH_3), 5.17 (2H, dd, J= 2.6, 0.62 Hz, H10), 7.83 (1H, t, J=0.53 Hz, H8). ^{13}C NMR (125.77 MHz, $CDCl_3$): δ= 27.96 (N1-CH_3), 29.79 (N3-CH_3), 36.44 (C10), 75.43 (C11), 76.07 (C12), 106.71 (C5), 140.42 (C8), 148.92 (C4), 151.60 (C2), 155.23 (C6). FT-IR/ATR vmax/cm^{-1}: 3243.55, 3111.71, 2946.11, 2127.13, 1703.88, 1651.15, 1543.95, 1477.34, 1437.21, 1373.59, 1232.32, 1190.89, 1025.01, 977.45, 744.20.

*3.1.2. 7-((1-benzyl-1H-1,2,3-triazol-4-yl) methyl)-1,3-dimethyl-3,7-dihydro-1H-purine-2,6–dione (**3**).*

A mixture of compound 2 (206 mg, 1mmol), sodium ascorbate (40 mg, 0.2 mmol), sodium azide (78 mg, 1.2 mmol), benzyl chloride (0.14 mL, 1.2 mmol), and Cu/Al mixed oxide (40 mg) in 6 mL of ethanol/water (3:1) were stirred at 80 °C for 30 min with microwave radiation. After this time, the Cu/Al mixed oxide is recovered by centrifugation and the supernatant is poured in 20 mL of water, extracted with dichloromethane, and dried over sodium sulfate anhydrous. Compound 3 is obtained, after chromatographic purification (CH_2Cl_2:EtOH 95:5), as a white powder: yield 78%, m.p. 169-171 °C. ^{1}H NMR (500.13 MHz, $CDCl_3$): δ= 3.38 (3H, s, N1-CH_3), 3.56 (3H, s, N3-CH_3), 5.49 (2H, s, H13), 5.56 (2H, s, H10), 7.26 (2H, m, H15), 7.36 (3H, m, H17, H16), 7.75 (1H, s, H12), 7.81 (1H, s, H8). ^{13}C NMR (125.77 MHz, $CDCl_3$): δ= 27.98 (N1-CH_3), 29.81 (N3-CH_3), 41.48 (C10), 54.32 (C13), 106.45 (C5), 123.48 (C12), 128.09 (C15), 128.89 (C17), 129.15 (C16), 134.23 (C14), 141.32 (C8), 142.52 (C11), 148.93 (C4), 151.58 (C2), 155.40 (C6). FT-IR/ATR vmax/cm^{-1}: 3114.70, 2957.28, 1690.39, 1650.26, 1546.81, 1453.58, 1214.63, 1021.75, 749.91. HRMS (ESI-TOF) (calculated for $C_{17}H_{18}N_7O_2$ + H+): 352.1516; found: 352.1514.

*3.1.3. 7-((1-(4-fluorobenzyl)-1H-1,2,3-triazol-4-yl) methyl)-1,3-dimethyl-3,7-dihydro-1H-purine-2,6-dione (**4**).*

Compound 4 was synthesized following the procedure described previously for compound 3, from compound 2 and 4-fluorobenzyl chloride. Compound 4 is obtained, after chromatographic purification (CH_2Cl_2:EtOH 95:5), as a white powder: yield 90%, m.p. 184-186 °C. ^{1}H NMR (400.13 MHz, $CDCl_3$): δ= 3.39 (3H, s, N1-CH_3), 3.56 (3H, s, N3-CH_3), 5.47 (2H, s, H13), 5.56 (2H, s, H10), 7.06 (2H, t, J= 8.61 Hz, H15), 7.26 (2H, dd, J= 8.64, 4.34 Hz, H16), 7.75 (1H, s, H12), 7.82 (1H, s, H8). ^{13}C NMR (100.61 MHz, $CDCl_3$): δ= 27.99 (N1-CH_3), 29.82 (N3-CH_3), 41.47 (C10), 53.58 (C13), 106.45 (C5), 116.09 (C15), 116.31 (C15), 123.39 (C12), 129.98 (C16), 130.06 (C16), 141.35 (C8), 142.65 (C11), 148.99 (C4), 151.59 (C2), 155.44 (C6), 161.69 (C14 or C17), 164.17 (C14 or C17). FT-IR/ATR vmax/cm^{-1}: 3144.88, 3116.27, 3000.48, 2960.31, 1691.08, 1651.91, 1549.09, 1512.06, 1456.51, 1226.98, 1023.54, 786.67, 750.59, 615.31, 522.38. HRMS (ESI-TOF) (calculated for $C_{17}H_{17}N_7O_2F$ + H+): 370.1422; found: 370.1419.

*3.1.4. 7-((1-(4-chlorobenzyl)-1H-1,2,3-triazol-4-yl) methyl)-1,3-dimethyl-3,7-dihydro-1H-purine-2,6-dione (**5**).*

Compound 5 was synthesized following the procedure described for compound 3, from compound 2 and 4-chlorobenzyl chloride. Compound 5 is obtained, after chromatographic purification (CH_2Cl_2: EtOH 95:5), as a light green powder: yield 76%, m.p. 194-196 °C. ^{1}H RMN (400.13 MHz, $CDCl_3$): δ= 3.39 (3H, s, N1-CH_3), 3.56 (3H, s, N3-CH_3), 5.47 (2H, s, H13), 5.56 (2H, s, H10), 7.20 (2H, d, J= 8.42 Hz, H15), 7.34 (2H, d, J= 842. Hz, H16), 7.77 (1H, s, H12), 7.82 (1H, s, H8). ^{13}C NMR (100.61 MHz, $CDCl_3$): δ= 27.98 (N1-CH_3), 29.81 (N3-CH_3), 41.45 (C10), 53.58 (C13), 106.45 (C5), 123.53 (C12), 129.38 (C15), 129.44 (C16), 132.72 (C14), 135.01 (C17), 141.36 (C8), 142.77 (C11), 149 (C4), 151.58 (C2), 155.44 (C6). FT-IR/ATR vmax/cm^{-1}: 3096.88, 3052.15, 2960.28, 1688.25, 1650.83, 1555.24, 1406.79, 1220.94, 1082.17, 1045.89, 978.31, 848.97, 785.63, 770.92, 608.01, 494.81. HRMS (ESI-TOF) (calculated for $C_{17}H_{17}N_7O_2Cl$ + H+): 386.1127; found: 386.1124.

*3.1.5. 7-((1-(4-bromobenzyl)-1H-1,2,3-triazol-4-yl) methyl)-1,3-dimethyl-3,7-dihydro-1H-purine-2,6-dione (**6**).*

Compound 6 was synthesized following the procedure described for compound 3, from compound 2 and 4-bromobenzyl bromide. Compound 6 is obtained, after chromatographic purification (CH_2Cl_2:EtOH 95:5), as a white powder: yield 63%, m.p. 199-201 °C. ^{1}H RMN (500.13 MHz, $CDCl_3$): δ= 3.39 (3H, s, N1-CH_3), 3.56 (3H, s, N3-CH_3), 5.45 (2H, s, H13), 5.56 (2H, s, H10), 7.13 (2H, d, J= 8.65 Hz, H15), 7.49 (2H, d, J= 8.61 Hz, H16), 7.76 (1H, s, H12), 7.80 (1H, s, H8). ^{13}C NMR (125.77 MHz, $CDCl_3$): δ= 27.96 (N1-CH_3), 29.79 (N3-CH_3), 41.46 (C10), 53.62 (C13), 106.45 (C5), 123.09 (C17), 123.49 (C12), 129.69 (C15), 132.33 (C16), 133.24 (C14), 141.31 (C8), 142.81 (C11), 149 (C4), 151.56 (C2), 155.42 (C6). FT-IR/ATR vmax/cm^{-1}: 3134.60, 3095.80, 3049.46, 2960.09, 1687.19, 1650.07, 1554.67, 1450.68, 1405.55, 1220.14, 1103.66, 1030.53, 978.62, 847.88, 607.67, 488.92. HRMS (ESI-TOF) (calculated for $C_{17}H_{17}N_7O_2Br$ + H+): 430.0621; found: 430.0618.

*3.1.6. 7-((1-(4-iodobenzyl)-1H-1,2,3-triazol-4-yl) methyl)-1,3-dimethyl-3,7-dihydro-1H-purine-2,6-dione (**7**).*

Compound 7 was synthesized following the procedure described for compound 3, from compound 2 and 4-iodobenzyl bromide. Compound 7 is obtained, after chromatographic purification (CH_2Cl_2:EtOH 95:5), as a white powder: yield 68%, m.p. 181-184 °C. ^{1}H NMR (400.13 MHz, $CDCl_3$): δ= 3.39 (3H, s, N1-CH_3), 3.56 (3H, s, N3-CH_3), 5.44 (2H, s, H13), 5.56 (2H, s, H10), 7.00 (2H, d, J= 8.38 Hz, H15), 7.69 (2H, d, J= 8.37 Hz, H16), 7.76 (1H, s, H12), 7.82 (1H, s, H8).^{13}C NMR (100.61 MHz, $CDCl_3$): δ= 28.02 (N1-CH_3), 29.84 (N3-CH_3), 41.46 (C10), 53.73 (C13), 94.76 (C17), 106.44 (C5), 123.54 (C12), 129.88 (C15), 133.88 (C14), 138.29 (C16), 141.35 (C8), 142.72 (C11), 148.98 (C4), 151.58 (C2), 155.43 (C6). FT-IR/ATR vmax/cm^{-1}: 3143.55, 3115.45, 2958.37, 1690.45, 1651.19, 1548.13, 1456.04, 1218.88, 1006.66, 750.30, 615.40, 498.95. HRMS (ESI-TOF) (calculated for $C_{17}H_{17}N_7O_2I$ + H+): 478.0483; found: 478.0478.

(6) The discussion on EIS measurements results should be rewritten. It is very shallow and should be expanded to convey meaning. Fundamental questions like the need of using constant phase element in the equivalent circuit need to be answered. Also for the purpose of clarity, the authors need to use appropriate scientific words to describe the technique. It is not clear what the authors meant by "the results were adjusted using equivalent electric circuits"

Reply: In the final version, we have modified the discussion in the results section.

4.1 OCP and EIS Electrochemical evaluation

Fig. 3a shows the variations in time of the open circuit potential (OCP) in static conditions at 50 ppm, at the electrode made of API 5L X52 steel in presence of different inhibitor concentrations. It should be mentioned that it was necessary the stabilization of the OCP previously to do the EIS determinations. The steady state was reached after 1700 seconds. Fig. 3b corresponds to the Nyquist diagram for the system without inhibitor, which depicts a depressed semicircle reaching a maximum Z_{real} value of 30 Ω cm^2 (adjusted with electrical circuit Figure 2a).
The Nyquist diagrams of each of the theophylline-triazoles are shown in Figs. 4a-4e. As can be seen, the diameter of the semicircle increases proportionally with the inhibitor's concentration. According to the shape of the semicircle, two time constant (using the circuit figure 2b) can be attributed, the charge transference resistance and the second to adsorbed molecules resistance [36-38]. The depressed semicircle is attributed due to frequency dispersion effect and surface irregularities and heterogeneities [39].

It can be observed that the Z_{real} value presents a large variation. Based on these results, it can be inferred that the presence of a halogen substituent in para position of the aromatic ring can modulate the inhibition capacity of the compound.
After obtaining the Nyquist diagrams of the compounds at different concentrations, the impedance results for API 5L X52 steel with and without inhibitor can be explained by an equivalent circuit (Figure 2) which comprise of R_{ct}

(charge transfer resistance), and Q is the constant phase element in parallel with Rs (solution resistance), R_{mol} is the molecules resistance.

Constant phase elements have widely been used [40] to account for deviations brought about by surface roughness. The impedance of CPE is given by the next equation [41]:

$$Z_{CPE} = Q^{-1}(j\omega)^{-n} \quad (1)$$

Where Y0 is the magnitude of the CPE, n the CPE exponent (phase shift), ω the angular frequency (ω=2πf, where f is the AC frequency), and *j* here is the imaginary unit. The capacity correction to its real values was calculated from Eq. (2), where ω_{max} is the frequency at which the imaginary part of the impedance ($-Z_{imag}$) has a maximum. C_{dl} represents the double layer capacitance (Eq. 2).

$$C_{\mathrm{dl}} = Y_0\left(\omega_m^{''}\right)^{n-1} \quad (2)$$

The value of inhibition efficiency (η) can be obtained by means of the following equation [42-43]:

$$\eta\,(\%) = \frac{\left(\frac{1}{Rp}\right)_{\mathrm{blank}} - \left(\frac{1}{Rp}\right)_{\mathrm{inhibitor}}}{\left(\frac{1}{Rp}\right)_{\mathrm{blank}}}\ x\ 100 \quad (3)$$

36. Obayes HR, Al-Amiery AA, Alwan G H, Amir A, Kadhum H, Mohamad A B. 2017. Sulphonamides as corrosion inhibitor: Experimental and DFT studies. *J. of Mol. Struct*. 1138, 27-34
37. Obot IB, Ankah NK, Sorour AA, Gasem ZM, Haruna K. 2017. 8-Hydroxyquinoline as an alternative green and sustainable acidizing oilfield corrosion inhibitor. *Sust. Mat. and Techn*., 14, 1-10
38. Pfeiffer M, Klock H, Helmut, Bergen G. Ehrenhaft, Ferreira P, Gollnick J., Fischer CB. 2017. Surface protection of low carbon steel with N-acyl sarcosine derivatives as green corrosion inhibitors. *Surf. Interfaces*, 9, 70-78.
39. Qiang Y, Zhang S, Yan S, Zou X, Chen S. 2017. Three indazole derivatives as corrosion inhibitors of copper in a neutral chloride solution. *Corros. Sci*. 126, 295-304.
40. Yadav M, Behera D, Sharma U. 2016. Nontoxic corrosion inhibitors for N80 steel in hydrochloric acid. *Arab. J. of Chem*., 9(2), s1487-s1495.
41. Mobin M, Basik M, Aslam J. 2018. Boswellia serrata gum as highly efficient and sustainable corrosion inhibitor for low carbon steel in 1 M HCl solution: Experimental and DFT studies. *J. Mol. Liq*., 263, 174–186
42 Javadian S, Yousefi A, Neshati J (2013) Synergistic effect of mixed cationic and anionic surfactants on the corrosion inhibitor behavior of mild steel in 3.5% NaCl. Appl. Surf. Sci., 285, 674–681.
43 Zarrouk A, Zarrok H, Ramli Y. (2016) Inhibitive properties, adsorption and theoretical study of 3,7-dimethyl-1-(prop-2-yn-1-yl)quinoxalin-2(1H)-one as efficient corrosion inhibitor for carbon steel in hydrochloric acid solution. J. Mol. Liq. 222, 239–252.

(7) The authors should also present the EIS results in Bode formats as the number of time constants is better revealed in Bode representation than in Nyquist representation.

Reply: Reply: We agree with this observation. Therefore, in the revised version we have included the bode plots.

…The Bode plots for API 5L X52 steel in the absence and presence of various concentrations of 1,2,3-triazoles 1,4-disubstited are represented in Fig. 5. An ideal capacitor is characterized by a fixed value of slope (unity) and phase angle (−90°). The increase in the values of phase angle in presence of different inhibitor concentrations suggest that

surface roughness of API 5L X52 steel decreased due to formation of protective film by theophylline-triazole derivative [43]. The result indicated that there was two-time constant coupled, and the system could be described by three resistances which consists of electrolyte resistance (R_s), charge transfer resistance (R_{ct}), organic molecules adsorbed resistance (R_{mol}) and double layer capacitance, as shown in Fig 2b. While, in absence inhibitor the phase angle vs log frequency show one time constant attributed to charge transfer resistance [44].
Finally, the corrosion inhibition effectiveness of 1,2,3-triazoles 1,4-disubstited can also be interpreted in the real impedance values axis of the Bode modulus plots which also increases as the concentration increase (Fig. 5 a,c, e, g and h)…

[43] Ebenso EE, Kabanda MM. 2012. Electrochemical and quantum chemical investigation of some azine and thiazine dyes as potential corrosion inhibitors for mild steel in hydrochloric acid solution. Ind. Eng. Chem. Res. 51, 12940–12958. *Ind. Eng. Chem. Res.* 51, 12940–12958.
[44] Zhang H, Pang X, Zhou M, Liu C, Wei L, Gao K. 2015. The behavior of pre-corrosion effect on the performance of imidazoline-based inhibitor in 3 wt.% NaCl solution saturated with CO_2, *Appl. Surf. Sci.* 356: 63–72.

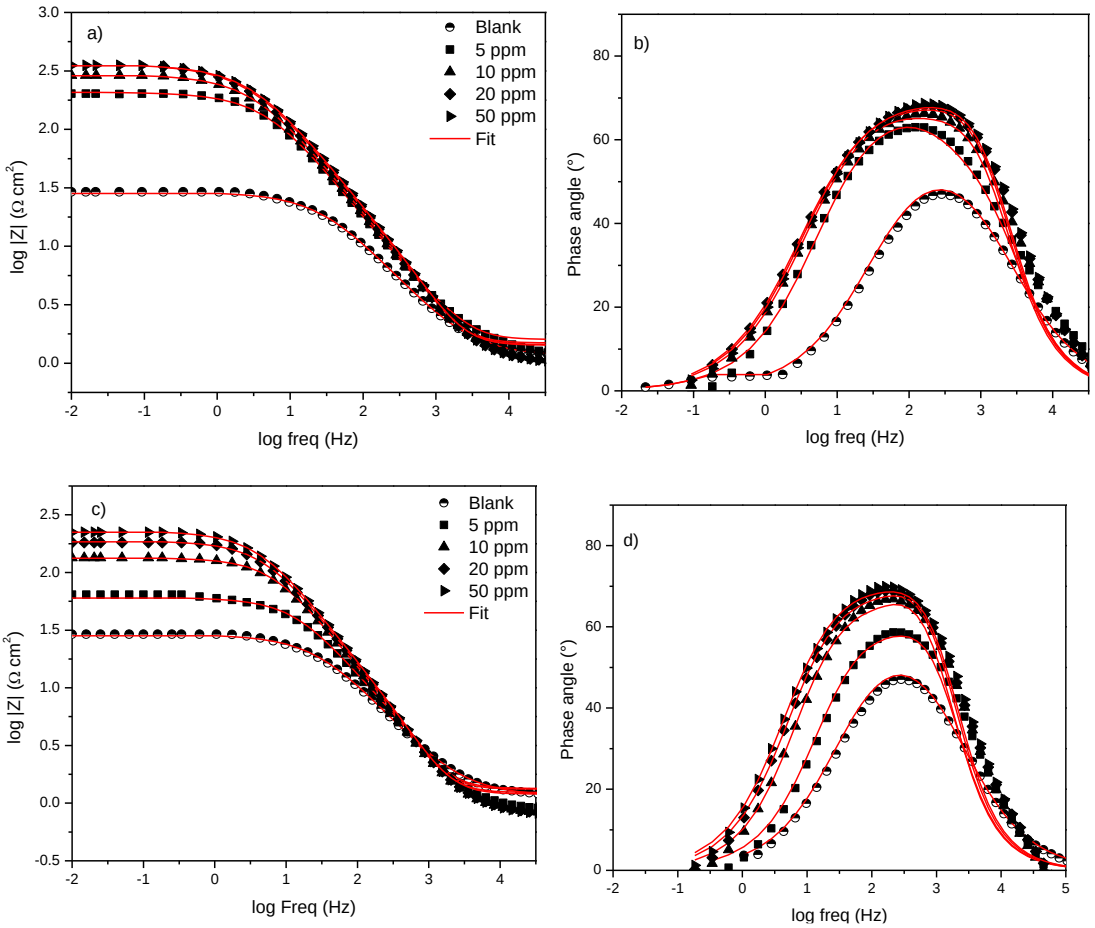

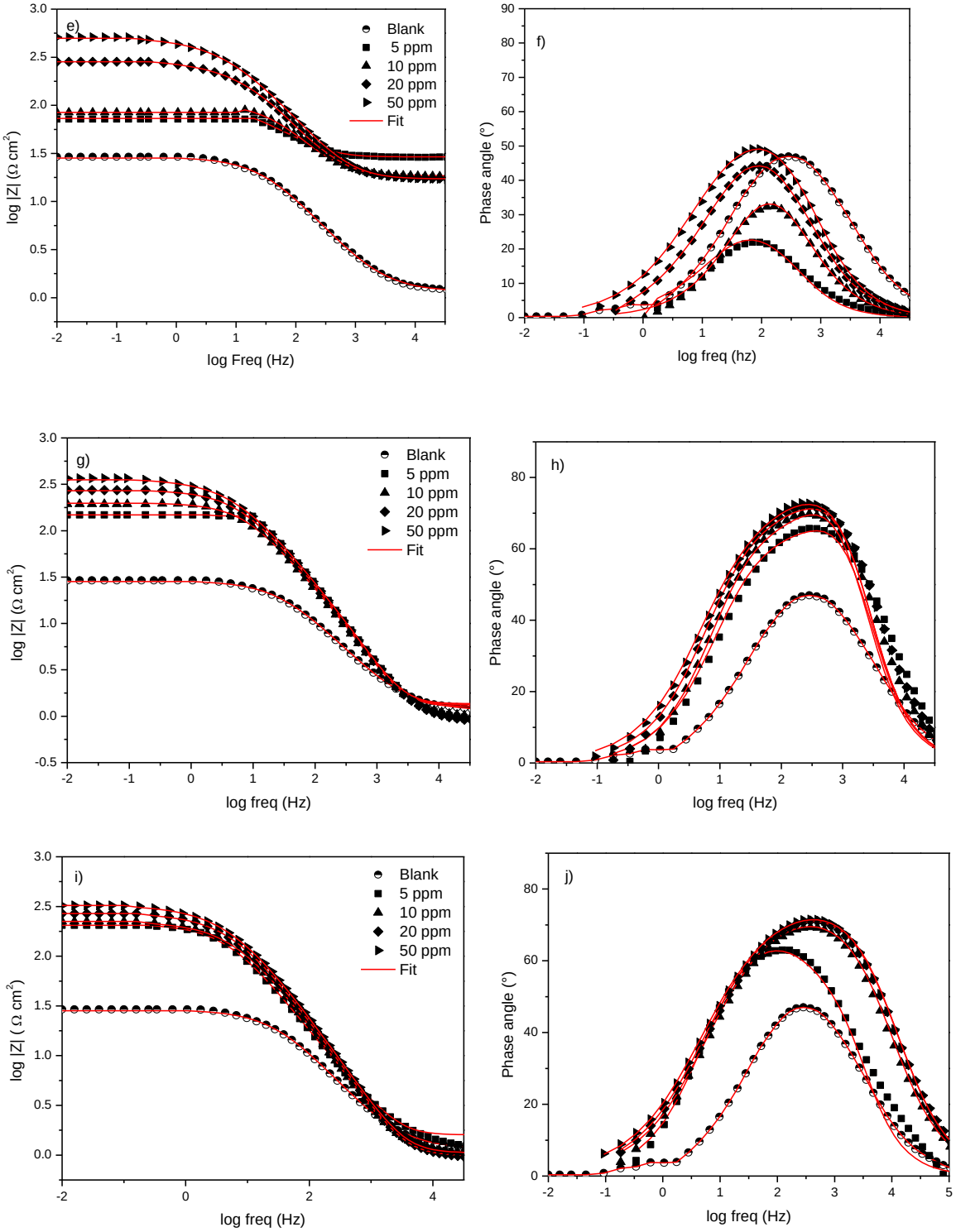

(8) Again, the discussion on potentiodynamic polarization technique should be rewritten as it is very shallow. The authors have not discussed the Fig.6 at all. The scope of the discussion should be expanded to make meaning.

Reply: We agree with this observation. The discussion on potentiodynamic polarization technique was added in the revised version as follows:

... Fig. 6 shows that all of the curves shift to a lower current density for both the anodic and cathodic half-reactions with the addition of 1,2,3-triazoles 1,4-disubstited in API 5L X52 steel immersed in HCl 1M, and the trend is more pronounced at 5 ppm inhibitor concentration; indicating that the anodic dissolution of API 5L X52 steel and cathodic reduction of hydrogen ions were inhibited [50].

This suggests that the rate of electrochemical reaction was reduced due to the formation of a protective layer of inhibitor molecules over the steel surface [51].

Furthermore, the cathodic Tafel curves are parallel (Fig. 5a and 5b), which shows that there is no change in the hydrogen evolution mechanism with the addition of 1,2,3-triazoles 1,4-disubstited. and the reduction of hydrogen ions mainly takes place through a charge transfer [52]…

[50] Quraishia MA, Lgazd H, Salghi R. 2018, Thiosemicarbazide and thiocarbohydrazide functionalized chitosan asecofriendly corrosion inhibitors for carbon steel in hydrochloric acid solution, *Int. J. Biol. Macrom*., 107,1747–1757.
[51] Stoyanova A, Petkova G, Peyerimhoff S, 2002, Correlation between the molecularstructure and the corrosion inhibiting effect of some pyrophthalonecompounds, *Chem. Phys.* 279 (1), 1–6.
[52] Solmaz R, Kardas G, Culha M, Yazıcı B, Erbil M, 2008, Investigation of adsorptionand inhibitive effect of 2-mercaptothiazoline on corrosion of mild steel inhydrochloric acid media, *Electrochim. Acta* 53 (20), 5941–5952.

(9) In Table 1, the authors should replace the SD with Chi squared values (values of goodness of fit) to ascertain the validity of the equivalent circuit used to fit the experimental data.

Reply: In final version, we changed the SD values with chi squared values

Table 1. *Electrochemical parameters of 1,2,3-triazoles 1,4-disubstituted in API 5L X52 steel immerse in HCl 1M*

Inhibitor	C (ppm)	Rs (Ω cm^2)	n	C_{dl} (μF cm^{-2})	R_{ct} (Ω cm^2)	R_{mol} (Ω cm^2)	η (%)	Chi squared
Blank	0	0.8	0.8	310.0	30	-	-	-
3	5	1.1	0.72	221.9	154.0	5.1	81.1	0.0833
	10	1.2	0.69	230.7	227.6	13.4	87.6	0.1119
	20	1.0	0.67	205.1	286.1	16.2	90.1	0.1130
	50	1.1	0.68	195.4	343.1	17.3	91.7	0.1052
4	5	1.1	0.73	228.9	49.9	9.6	49.6	0.1447
	10	1.3	0.75	192.8	112.4	18.9	77.2	0.1672
	20	1.2	0.72	193.4	168.1	19.5	84.0	0.1415
	50	1.2	0.71	182.7	210.4	18.6	86.9	0.1366
5	5	11.5	0.74	247.3	35.4	36.8	58.4	0.0020
	10	8.0	0.88	214.8	68.1	16.7	64.6	0.0016
	20	8.5	0.95	170.8	265.7	5.4	88.9	0.0017
	50	6.3	0.62	89.9	492.8	6.7	94.0	0.0014
6	5	1.0	0.70	174.4	134.5	14.4	79.9	0.1245
	10	1.1	0.72	129.4	169.8	29.8	85.0	0.0893
	20	1.1	0.68	123.2	248.4	28.7	89.2	0.1065
	50	1.2	0.63	108.2	335.3	29.5	91.8	0.1065
7	5	1.5	0.70	172.7	201.8	5.1	85.5	0.0024
	10	1.0	0.65	153.4	224.1	0.5	86.6	0.0036
	20	0.9	0.63	158.1	272.4	2.6	89.1	0.0045
	50	1.0	0.60	153.2	328.2	2.9	90.9	0.0040

(10) The units of bc and ba are not correct. The units should be mV/dec

Reply: We agree with this observation. In the final version, we changed the units as follows:

Table 2. Electrochemical parameters obtained by means of polarization curves for 1,2,3-triazoles 1,4-disubstited in API 5L X52 steel immerse in HCl 1M

Inhibitor	*C* (ppm)	E_{corr} (mV) vs Ag/AgCl	bc (mV dec^{-1})	ba (mV dec^{-1})	i_{corr} (mA/cm^2)	η_{pol} (%)
Blank	0	-421.2	-106.5	84.6	0.32	-
3	5	-450.8	-107.0	54.3	0.04	87.3
3	50	-470.1	-109.5	75.0	0.04	86.9
4	5	-448.0	-163.4	80.4	0.08	76.6
4	50	-439.9	-158.8	74.7	0.04	87.0
5	5	-447.6	-146.8	52.6	0.07	79.4
5	50	-441.0	-110.2	66.3	0.02	71.0
6	5	-413.4	-122.1	30.5	0.02	94.3
6	50	-427.2	-136.2	48.4	0.02	93.5
7	5	-410.8	-161.2	52.1	0.03	90.3
7	50	-425.3	-132.2	69.5	0.04	88.2

(11) In Table 3, the authors should the replace linear regression equation with values of the slopes. Also values of Kads and not ln Kads should be given.

Reply: We agree with this suggestion thus Table 3 has been modified accordingly.

Table 3. Adjustment of thermodynamic data with the Langmuir isotherm

Compound	Kads	ΔG° ads (kJ mol^{-1})	Slopes (M)	R^2
3	2.66×10^7	-41.7	C / θ =1.0.759C	0.9982
4	5.95×10^6	-38.1	C / θ =1.0788C	0.9979
5	5.38×10^6	-37.8	C / θ =0.9749C	0.9965
6	2.66×10^7	-41.7	C / θ =1.0700C	0.9998
7	5.37×10^7	-43.4	C / θ =1.0895C	0.9989

(12) Finally the English language of this manuscript is very poor and need serious improvement. The assistance of native English speakers may be sought in this regards.

Reply: The English of the manuscript was thoroughly revised.

ROYAL SOCIETY OPEN SCIENCE

R. Soc. open sci.
doi:10.1098/not yet assigned

Adsorption and corrosion inhibition behavior of new theophylline-triazole based derivatives for steel in acidic medium

Araceli Espinoza-Vázquez[a], Francisco Javier Rodríguez-Gómez[a], Ivonne Karina Martínez-Cruz[b], Deyanira Ángeles-Beltrán,[b], Guillermo E. Negrón-Silva[b*], Manuel Palomar-Pardavé,[c] Leticia Lomas Romero,[c] Diego Pérez-Martínez[c], Alejandra M. Navarrete-López[b]

[a]Facultad de Química, Departamento de Ingeniería Metalúrgica, Universidad Nacional Autónoma de México, Av. Universidad No. 3000, Coyoacán, C.U., Ciudad de México, C.P. 04510, México.

[b]Departamento de Ciencias Básicas, Universidad Autónoma Metropolitana-Azcapotzalco, Av. San Pablo No. 180, Ciudad de México, C.P. 02200, México

[c]Departamento de Materiales, Universidad Autónoma Metropolitana-Azcapotzalco, Av. San Pablo No. 180, Ciudad de México, C.P. 02200, México. [d]Departamento de Química, Universidad Autónoma Metropolitana-Iztapalapa, Av. San Rafael Atlixco No. 186, Ciudad de México, C.P. 09340, México.

Keywords: Theophylline, corrosion inhibition, API 5L X52 steel, acid, quantum chemical calculation

1. Summary

The design and synthesis of a series of theophylline derivatives containing 1,2,3-triazole moieties is presented. The corrosion inhibition activities of these new triazole-theophylline compounds were evaluated by studying the corrosion of API 5L X52 steel in 1 M HCl media. The results showed that an increase in the concentration of the theophylline-triazole derivatives also increases the charge transference resistance (R_{ct}) value, enhancing inhibition efficiency and decreasing the corrosion process. The electrochemical impedance spectroscopy under static conditions studies revealed that the best inhibition efficiencies (~90%) at 50 ppm are presented by the all- substituted compounds. According to the Langmuir isotherm, the compounds 4 and 5 analyzed exhibit physisorption-chemisorption process, with exception of the hydrogen 3, bromo 6 and iodo 7 substituted compound, which exhibit chemisorption process. The corrosion when submerging a steel bar in 1 M HCl was studied using SEM-EDS. This experiment showed that the corrosion process decreases considerably in the presence of 50 ppm of the organic inhibitors. Finally, theoretical study showed a correlation between EHOMO, hardness (η), electrophilicity (W), atomic charge and the inhibition efficiency in which the iodo 7 substituted compound presents the best inhibitor behavior.

2. Introduction

*Author for correspondence (gns@azc.uam.mx).

†Present address: Departamento de Ciencias Básicas, Universidad Autónoma Metropolitana-Azcapotzalco, Av. San Pablo No. 180, Ciudad de México, C.P. 02200, México

Steel corrosion remains as one of the most significant problem to industry. This naturally occurring phenomenon, that takes place at the metal-solution interface, substantially decrease the life of the equipment and facilitates the dissolution of environmentally toxic metal from the components [1-3]. In this regard, several organic molecules are recognized as corrosion inhibitors for a number of metals and alloys [4-6]. The adsorption of organic molecules at the metal surface both disrupts the properties of the metal/solution interface, effectively inhibiting the corrosion process [7], and eliminates the need for expensive and toxic inhibitor compounds [8].

It has been found that molecules with lone electron pairs and/or π-electrons in their structure shows great affinity to be adsorbed into the metallic material [9-12]. Thus, heterocycles containing nitrogen, oxygen, sulfur, and unsaturation in its structure are excellent candidates to be evaluated as corrosion inhibitors. In this context, nitrogen-containing heterocycles have been regarded as the most effective corrosion inhibitors of steel in acid solutions [13, 14].

Additionally, to their biological activities [15-21] nitrogen-containing heterocycles derived from xanthine, such as theophylline and theobromine (although these promote corrosion under certain conditions) [22, 23]. The caffeine, have demonstrated to possess great activity as corrosion inhibitors for a series of metals and alloys.

Recently, theophylline has been studied as a corrosion inhibitor using an API 5L X70 steel and proved effective at low concentrations [24].

On the other hand, the triazole derivatives are another class of nitrogen-containing heterocycles that have drawn attention for their potential applications in pharmaceutics, coordination chemistry and as corrosion inhibitors. Several reports have highlighted the capabilities of these compounds to strongly adsorb on metal surfaces, achieving an adequate corrosion inhibition efficiency at low concentrations [25-32].

A typical pathway to enhance the corrosion inhibition efficiency of a given heterocycle is to modify its structure with various substituents or functional groups. Moreover, a synergistic effect could be achieved if those substituents possess corrosion inhibition activity by themselves. Accordingly, this work presents the design and synthesis of new theophylline derivatives bearing 1,2,3-triazole moieties, those corrosion inhibitors that are easy to prepare and low cost. These novel compounds were tested as corrosion inhibition species in order to establish structure-activity relationships and to gain further insight into their adsorption properties and the steel protection.

3. Materials and Methods

3.1. Synthesis of the theophylline-triazole inhibitors (Figure 1)

*3.1.1. 1,3-dimethyl-7-(prop-2-in-1-yl)-3,7-dihydro-1H-purine-2,6-dione (**2**).*

Compound 2 was synthesized following the procedure described by Ruddarraju et al [21]. A mixture of theophylline (1) (1.98 g, 11 mmol) and potassium carbonate (1.990 g, 14.4 mmol) in DMF (30 mL) were stirred vigorously at room temperature for 20 minutes. After this time, propargyl bromide (1.68 mL, 22.2 mmol) was added and temperature was increased at 85 °C with vigorous stirring for another 2 h. Then, the mixture was poured in cold water. The compound was recovered as a white powder: yield 80%, m.p. 220-222 °C. ^{1}H NMR (500.13 MHz, $CDCl_3$): δ (ppm)= 2.60 (1H, t, J=2.61 Hz, H12), 3.41 (3H, s, N1-CH_3), 3.60 (3H, s, N3-CH_3), 5.17 (2H, dd, J= 2.6, 0.62 Hz, H10), 7.83 (1H, t, J=0.53 Hz, H8). ^{13}C NMR (125.77 MHz, $CDCl_3$): δ= 27.96 (N1-CH_3), 29.79 (N3-CH_3), 36.44 (C10), 75.43 (C11), 76.07 (C12), 106.71 (C5), 140.42 (C8), 148.92 (C4), 151.60 (C2), 155.23 (C6). FT-IR/ATR vmax/cm^{-1}: 3243.55, 3111.71, 2946.11, 2127.13, 1703.88, 1651.15, 1543.95, 1477.34, 1437.21, 1373.59, 1232.32, 1190.89, 1025.01, 977.45, 744.20.

*3.1.2. 7-((1-benzyl-1H-1,2,3-triazol-4-yl) methyl)-1,3-dimethyl-3,7-dihydro-1H-purine-2,6–dione (**3**).*

A mixture of compound 2 (206 mg, 1mmol), sodium ascorbate (40 mg, 0.2 mmol), sodium azide (78 mg, 1.2 mmol), benzyl chloride (0.14 mL, 1.2 mmol), and Cu/Al mixed oxide (40 mg) in 6 mL of ethanol/water (3:1) were stirred at 80 °C for 30 min with microwave radiation. After this time, the Cu/Al mixed oxide is recovered by centrifugation

and the supernatant is poured in 20 mL of water, extracted with dichloromethane, and dried over sodium sulfate anhydrous. Compound 3 is obtained, after chromatographic purification (CH_2Cl_2:EtOH 95:5), as a white powder: yield 78%, m.p. 169-171 °C. ^{1}H NMR (500.13 MHz, $CDCl_3$): δ= 3.38 (3H, s, N1-CH_3), 3.56 (3H, s, N3-CH_3), 5.49 (2H, s, H13), 5.56 (2H, s, H10), 7.26 (2H, m, H15), 7.36 (3H, m, H17, H16), 7.75 (1H, s, H12), 7.81 (1H, s, H8). ^{13}C NMR (125.77 MHz, $CDCl_3$): δ= 27.98 (N1-CH_3), 29.81 (N3-CH_3), 41.48 (C10), 54.32 (C13), 106.45 (C5), 123.48 (C12), 128.09 (C15), 128.89 (C17), 129.15 (C16), 134.23 (C14), 141.32 (C8), 142.52 (C11), 148.93 (C4), 151.58 (C2), 155.40 (C6). FT-IR/ATR vmax/cm^{-1}: 3114.70, 2957.28, 1690.39, 1650.26, 1546.81, 1453.58, 1214.63, 1021.75, 749.91. HRMS (ESI-TOF) (calculated for $C_{17}H_{18}N_7O_2$ + H+): 352.1516; found: 352.1514.

*3.1.3. 7-((1-(4-fluorobenzyl)-1H-1,2,3-triazol-4-yl) methyl)-1,3-dimethyl-3,7-dihydro-1H-purine-2,6-dione (**4**).*

Compound 4 was synthesized following the procedure described previously for compound 3, from compound 2 and 4-fluorobenzyl chloride. Compound 4 is obtained, after chromatographic purification (CH_2Cl_2:EtOH 95:5), as a white powder: yield 90%, m.p. 184-186 °C. ^{1}H NMR (400.13 MHz, $CDCl_3$): δ= 3.39 (3H, s, N1-CH_3), 3.56 (3H, s, N3-CH_3), 5.47 (2H, s, H13), 5.56 (2H, s, H10), 7.06 (2H, t, J= 8.61 Hz, H15), 7.26 (2H, dd, J= 8.64, 4.34 Hz, H16), 7.75 (1H, s, H12), 7.82 (1H, s, H8). ^{13}C NMR (100.61 MHz, $CDCl_3$): δ= 27.99 (N1-CH_3), 29.82 (N3-CH_3), 41.47 (C10), 53.58 (C13), 106.45 (C5), 116.09 (C15), 116.31 (C15), 123.39 (C12), 129.98 (C16), 130.06 (C16), 141.35 (C8), 142.65 (C11), 148.99 (C4), 151.59 (C2), 155.44 (C6), 161.69 (C14 or C17), 164.17 (C14 or C17). FT-IR/ATR vmax/cm^{-1}: 3144.88, 3116.27, 3000.48, 2960.31, 1691.08, 1651.91, 1549.09, 1512.06, 1456.51, 1226.98, 1023.54, 786.67, 750.59, 615.31, 522.38. HRMS (ESI-TOF) (calculated for $C_{17}H_{17}N_7O_2F$ + H+): 370.1422; found: 370.1419.

*3.1.4. 7-((1-(4-chlorobenzyl)-1H-1,2,3-triazol-4-yl) methyl)-1,3-dimethyl-3,7-dihydro-1H-purine-2,6-dione (**5**).*

Compound 5 was synthesized following the procedure described for compound 3, from compound 2 and 4-chlorobenzyl chloride. Compound 5 is obtained, after chromatographic purification (CH_2Cl_2: EtOH 95:5), as a light green powder: yield 76%, m.p. 194-196 °C. ^{1}H RMN (400.13 MHz, $CDCl_3$): δ= 3.39 (3H, s, N1-CH_3), 3.56 (3H, s, N3-CH_3), 5.47 (2H, s, H13), 5.56 (2H, s, H10), 7.20 (2H, d, J= 8.42 Hz, H15), 7.34 (2H, d, J= 842. Hz, H16), 7.77 (1H, s, H12), 7.82 (1H, s, H8). ^{13}C NMR (100.61 MHz, $CDCl_3$): δ= 27.98 (N1-CH_3), 29.81 (N3-CH_3), 41.45 (C10), 53.58 (C13), 106.45 (C5), 123.53 (C12), 129.38 (C15), 129.44 (C16), 132.72 (C14), 135.01 (C17), 141.36 (C8), 142.77 (C11), 149 (C4), 151.58 (C2), 155.44 (C6). FT-IR/ATR vmax/cm^{-1}: 3096.88, 3052.15, 2960.28, 1688.25, 1650.83, 1555.24, 1406.79, 1220.94, 1082.17, 1045.89, 978.31, 848.97, 785.63, 770.92, 608.01, 494.81. HRMS (ESI-TOF) (calculated for $C_{17}H_{17}N_7O_2Cl$ + H+): 386.1127; found: 386.1124.

*3.1.5. 7-((1-(4-bromobenzyl)-1H-1,2,3-triazol-4-yl) methyl)-1,3-dimethyl-3,7-dihydro-1H-purine-2,6-dione (**6**).*

Compound 6 was synthesized following the procedure described for compound 3, from compound 2 and 4-bromobenzyl bromide. Compound 6 is obtained, after chromatographic purification (CH_2Cl_2:EtOH 95:5), as a white powder: yield 63%, m.p. 199-201 °C. ^{1}H RMN (500.13 MHz, $CDCl_3$): δ= 3.39 (3H, s, N1-CH_3), 3.56 (3H, s, N3-CH_3), 5.45 (2H, s, H13), 5.56 (2H, s, H10), 7.13 (2H, d, J= 8.65 Hz, H15), 7.49 (2H, d, J= 8.61 Hz, H16), 7.76 (1H, s, H12), 7.80 (1H, s, H8). ^{13}C NMR (125.77 MHz, $CDCl_3$): δ= 27.96 (N1-CH_3), 29.79 (N3-CH_3), 41.46 (C10), 53.62 (C13), 106.45 (C5), 123.09 (C17), 123.49 (C12), 129.69 (C15), 132.33 (C16), 133.24 (C14), 141.31 (C8), 142.81 (C11), 149 (C4), 151.56 (C2), 155.42 (C6). FT-IR/ATR vmax/cm^{-1}: 3134.60, 3095.80, 3049.46, 2960.09, 1687.19, 1650.07, 1554.67, 1450.68, 1405.55, 1220.14, 1103.66, 1030.53, 978.62, 847.88, 607.67, 488.92. HRMS (ESI-TOF) (calculated for $C_{17}H_{17}N_7O_2Br$ + H+): 430.0621; found: 430.0618.

*3.1.6. 7-((1-(4-iodobenzyl)-1H-1,2,3-triazol-4-yl) methyl)-1,3-dimethyl-3,7-dihydro-1H-purine-2,6-dione (**7**).*

Compound 7 was synthesized following the procedure described for compound 3, from compound 2 and 4-iodobenzyl bromide. Compound 7 is obtained, after chromatographic purification (CH_2Cl_2:EtOH 95:5), as a white powder: yield 68%, m.p. 181-184 °C. ^{1}H NMR (400.13 MHz, $CDCl_3$): δ= 3.39 (3H, s, N1-CH_3), 3.56 (3H, s, N3-CH_3), 5.44 (2H, s, H13), 5.56 (2H, s, H10), 7.00 (2H, d, J= 8.38 Hz, H15), 7.69 (2H, d, J= 8.37 Hz, H16), 7.76 (1H, s, H12), 7.82 (1H, s, H8).^{13}C NMR (100.61 MHz, $CDCl_3$): δ= 28.02 (N1-CH_3), 29.84 (N3-CH_3), 41.46 (C10), 53.73 (C13), 94.76 (C17), 106.44 (C5), 123.54 (C12), 129.88 (C15), 133.88 (C14), 138.29 (C16), 141.35 (C8), 142.72 (C11), 148.98 (C4), 151.58 (C2),

155.43 (C6). FT-IR/ATR vmax/cm^{-1}: 3143.55, 3115.45, 2958.37, 1690.45, 1651.19, 1548.13, 1456.04, 1218.88, 1006.66, 750.30, 615.40, 498.95. HRMS (ESI-TOF) (calculated for $C_{17}H_{17}N_7O_2I$ + H+): 478.0483; found: 478.0478.

3.2. Corrosion inhibition tests

3.2.1 API 5L X52 steel

API 5L X52 steel was used for the corrosion inhibition studies. This type of steel has a metallographic preparation with the following nominal composition (wt%): C, 0.025; Mn, 1.65; Si, 0.26; Ti, 0.015; V, 0.001; Nb, 0.068; Mo, 0.175; S, 0.0025; Al, 0.045; Ni, 0.08; Cr, 0.07; Cu, 0.21; and balance iron.

3.2.2 Inhibitor solutions

A 0.01 M solution of each theophylline-triazole inhibitor 3–7 in DMF was prepared. Then, concentrations of 5, 10, 20 and 50 ppm of the inhibitor were added to the 1 M HCl corrosive solution.

3.2.3. Characterization of surfaces by SEM-EDS

The API 5L X52 steel surface was prepared both without (blank) and with inhibitor; a 50-ppm concentration was used for a 24 h immersion time. After that experiment, the steel was washed with distilled water, dried, and the surface analysed using a Zeiss SUPRA 55 VP electronic sweep microscope at 10 kV with a 300x secondary electron detector.

3.2.4. Electrochemical evaluation

The potential was stabilized at 20 °C for approximately 1800 s before electrochemical impedance spectroscopy (EIS) test. EIS: a sinusoidal potential of ±10 mV was applied in a frequency interval of 10^{-2} Hz to 10^4 Hz, in an electrochemical cell with three electrodes using Gill Ac. The working electrode was API 5L X52 steel, while reference electrode and counter electrode were Ag/AgCl saturated with chloride potassium and graphite respectively. The electrode surface was prepared using conventional metallography methods over an exposed area of 1 cm^2. After EIS measurements, the potentiodynamic polarization curves of 5 and 50 ppm of inhibitors were obtained. The measurements covered a range from -500 mV to 500 mV regarding the open circuit potential (OCP), with a sweep velocity of 60 mV min^{-1} using the ACM Analysis software for data interpretation.

3.2.5. Theoretical assessment

The calculations have been performed with Gaussian09 [33] using the M06-2X functional [34] and LANL2DZ basis set. For Cl, Br and I the LANL2 effective core potential was coupled with the LANL2DZ basis set. Frequency calculations were executed in order to guarantee the minimal energy structure. The solvent (water) effect is including with the Solvation Model based on Density (SMD) [35].

4. Results and Discussion

4.1 OCP and EIS Electrochemical evaluation

Fig. 3a shows the variations in time of the open circuit potential (OCP) in static conditions at 50 ppm, at the electrode made of API 5L X52 steel in presence of different inhibitor concentrations. It should be mentioned that it was necessary the stabilization of the OCP previously to do the EIS determinations. The steady state was reached after 1700 seconds. Fig. 3b corresponds to the Nyquist diagram for the system without inhibitor, which depicts a depressed semicircle reaching a maximum Z_{real} value of 30 Ω cm^2 (adjusted with electrical circuit Figure 2a).

The Nyquist diagrams of each of the theophylline-triazoles are shown in Figs. 4a-4e. As can be seen, the diameter of the semicircle increases proportionally with the inhibitor's concentration. According to the shape of the semicircle, two time constant (using the circuit figure 2b) can be attributed, the charge transference resistance and the second to adsorbed molecules resistance [36-38]. The depressed semicircle is attributed due to frequency dispersion effect and surface irregularities and heterogeneities [39].

It can be observed that the Z_{real} value presents a large variation. Based on these results, it can be inferred that the presence of a halogen substituent in para position of the aromatic ring can modulate the inhibition capacity of the compound.

After obtaining the Nyquist diagrams of the compounds at different concentrations, the impedance results for API 5L X52 steel with and without inhibitor can be explained by an equivalent circuit (Figure 2) which comprise of R_{ct} (charge transfer resistance), and Q is the constant phase element in parallel with Rs (solution resistance), R_{mol} is the molecules resistance.

Constant phase elements have widely been used [40] to account for deviations brought about by surface roughness. The impedance of CPE is given by the next equation [41]:

$$Z_{CPE} = Q^{-1}(j\omega)^{-n} \quad (1)$$

Where Y0 is the magnitude of the CPE, n the CPE exponent (phase shift), ω the angular frequency (ω=2πf, where f is the AC frequency), and j here is the imaginary unit. The capacity correction to its real values was calculated from Eq. (2), where ω_{max} is the frequency at which the imaginary part of the impedance ($-Z_{imag}$) has a maximum. C_{dl} represents the double layer capacitance (Eq. 2).

$$C_{dl} = Y_0(\omega''_m)^{n-1} \quad (2)$$

The value of inhibition efficiency (η) can be obtained by means of the following equation [42-43]:

$$\eta\,(\%) = \frac{\left(\frac{1}{Rp}\right)\text{blank} - \left(\frac{1}{Rp}\right)\text{inhibitor}}{\left(\frac{1}{Rp}\right)\text{blank}}\, x\, 100 \quad (3)$$

The Bode plots for API 5L X52 steel in the absence and presence of various concentrations of 1,2,3-triazoles 1,4-disubstited are represented in Fig. 5. An ideal capacitor is characterized by a fixed value of slope (unity) and phase angle (−90°). The increase in the values of phase angle in presence of different inhibitor concentrations suggest that surface roughness of API 5L X52 steel decreased due to formation of protective film by theophylline-triazole derivative [44]. The result indicated that there was two-time constant coupled, and the system could be described by three resistances which consists of electrolyte resistance (R_s), charge transfer resistance (R_{ct}), organic molecules adsorbed resistance (R_{mol}) and double layer capacitance, as shown in Fig 2b. While, in absence inhibitor the phase angle vs log frequency show one time constant attributed to charge transfer resistance [45].

Finally, the corrosion inhibition effectiveness of 1,2,3-triazoles 1,4-disubstited can also be interpreted in the real impedance values axis of the Bode modulus plots which also increases as the concentration increase (Fig. 5 a,c, e, g and h).

In the electrochemical parameters obtained from the adjustment of experimental data with the equivalent circuit shown previously, it is possible to notice that the value of the capacitance of the electrochemical double layer (C_{dl}) decreases when more concentration of the inhibitor is added, due to the gradual displacement of water molecules with the theophylline-triazole inhibitor molecules in the working electrode, which decreases the number of active sites and consequently delays the corrosion phenomenon [46-47]. The charge transference resistance (R_{ct}) also increases when more concentration of the inhibitor is added in every case. Finally, the value of the inhibition efficiency reached a maximum of 94% of effectivity at 50 ppm for the compound containing chloride in its chemical structure.

In Fig. 6, a comparative of inhibition efficiency values for each theophylline-triazole derivative is shown. It is important to mention that, for the lowest concentration measurements (5 ppm), the best inhibition efficiency is presented by compound **7**.
The presence of the halogen attached to the benzene ring does not show a clear trend in the improvement of the inhibition efficiency, because it is not the only fragment that is interacting with the metal surface [48]. With respect to the highest inhibitor concentration (50 ppm), the best inhibition efficiency is presented by compound **5** (η (%) = 94), followed closely by compound **3** and **6** (η (%) ~ 91). The best inhibitor (compound 5) can be attributed to the increased electron affinity of Cl, that could create a partially negative charge that can interact more efficiently with the positively charged metal surface, enhancing the overall adsorption of the molecule and thus, increasing its corrosion inhibition efficiency.
Also, worth to mention is the fact that the corrosion inhibition efficiency of all of the theophylline-triazole derivatives is higher than the corrosion inhibition observed in the underivatized theophylline [23] but is comparatively lower than other 1,2,3-triazole derivatives reported earlier [28-30]

4.2 Potentiodynamic polarization evaluation

The potentiodynamic polarization curves of the API 5L X52 steel immerse in HCl 1M in absence and presence of triazoles 1,4-disubstituted (5 and 50 ppm) are shown in Fig. 7.

The parameters as the corrosion potential (E_{corr}), Tafel anodic pendant (ba), cathodic pendant (bc), and corrosion current density (i_{corr}) obtained from the curves are shown in Table 2.
The inhibition efficiency (η_{pol}) is calculated with the following equation [49-50]:

$$\eta_{pol}(\%) = \frac{i_{corr\ blank} - i_{corr\ inhibitor}}{i_{corr\ blank}} \text{ x } 100 \quad (4)$$

Where *i*corr is the corrosion current density in absence and presence of the inhibitor.

Fig. 7 shows that all of the curves move to lower current densities for both the anodic and cathodic half-reactions with the addition of 1,2,3-triazoles 1,4-disubstited in API 5L X52 steel immersed in HCl 1M, and the trend is more pronounced at 5 ppm inhibitor concentration; indicating that the anodic dissolution of API 5L X52 steel and cathodic reduction of hydrogen ions were inhibited [51].
This suggests that the rate of electrochemical reaction was reduced due to the formation of a protective layer of inhibitor molecules over the steel surface [52].
Furthermore, the cathodic Tafel curves are parallel (Fig. 7a and 7b), which shows that there is no change in the hydrogen evolution mechanism with the addition of 1,2,3-triazoles 1,4-disubstited. and the reduction of hydrogen ions mainly takes place through a charge transfer [53].
In Table 2, the electrochemical parameters are summarized. As can be seen, the corrosion current density decreases as the inhibition efficiency increases, which is attributed to the adsorption of the organic compound on the metal surface in HCl 1M, generating a blockage of the active sites [54-55].
On the other hand, the corrosion potential (E_{corr}) is lesser than 85 mV, which suggests that it belongs to the mixed type with cathodic predominance for the two concentrations studied [56].
It is worth noting that the inhibition efficiency was also calculated by this technique for two concentrations of each organic compound (summarized in Table 2), which closely correlate with the results obtained by the EIS technique.

4.3 Adsorption Isotherm

Among all of the adsorption mechanism descriptions reported in the literature [57-60], the most common model to describe this process is Langmuir's isotherms (equation 5). The corresponding adjustment for this model was performed, and the adjustment parameters are shown in Table 3.

$$\frac{C}{\theta} = \frac{1}{K_{ads}} + C \quad (5)$$

Where C is the concentration, θ is the coating degree and K_{ads} is the adsorption constant.

The value of K_{ads} is related with the Gibbs free energy value ($\Delta G°_{ads}$) and is related to the following equation [61]:

$$\Delta G^{\circ}_{ads} = -RT\ln(55.5\,K_{ads}) \quad (6)$$

Where the numeric value of 55.5 is the molar concentration of water in an acid solution, R is the constant of ideal gasses and T is the absolute temperature of the system.
The calculated values of the thermodynamic adjustment are also shown in Table 3. Several authors mention that the values of ΔG° ads around -40 KJ/mol or more negative are consistent with the charge interchange between the metal and the organic compound, so the reaction is defined as a chemisorption, while the values of ΔG° ads lower than -20 KJ/mol produce only an electrostatic interaction (physisorption) [62-63].
According to these results, the compounds 3, 6 and 7 presents chemisorption process and, for the rest of the compounds, a physisorption-chemisorption type process is observed (Figure 8)[64-66].

4.4 Adsorption mechanism

The corrosion inhibition of API 5L X52 in HCl 1M provoked by 1,2,3-triazoles 1,4-disubstited molecules can be explained as follows (Figure 9): The protonated species of the organic compounds interact, throughout Columbic forces, with previously adsorbed chlorides ions (Cl-) present on the API 5L X52 steel surface which results in physisorption of the inhibitor molecules. This way, the inhibitor molecules compete with H^+ for electrons on steel surfaces [67]. Moreover, the donation of lone electrons pairs of nitrogen atoms to the empty orbital of Fe atoms would induce a chemisorption process of the organic molecule [68] and the accumulation of negative charges on the steel surface can be transferred from the d orbital of Fe to unoccupied $\pi*$ (anti-bonding) of 1,2,3-triazoles 1,4-disubstited molecules (retro-donation) [69], see Figure 9a and 9b. The combination of these two types of adsorption mechanisms is carried out for the compounds evaluated. However, the compound 7 (Figure 9b) showed a stronger interaction (chemisorption) by nitrogen heteroatoms that have free electron pairs with steel, demonstrated with thermodynamic analysis using the Langmuir model.

4.5 SEM-EDS Surface analysis

The surfaces of the API 5L X52 steel with and without inhibitor (fig. 10), were characterized by SEM- EDS to corroborate the effectiveness of the inhibitor by evaluating the electrochemical response. Figure 10a shows the surface of polished steel, while in figure 10c, shows the steel surface after 24 hours of immersion in a solution 1M HCl. As can be seen, the metallic surface presents damage due to the presence of chloride ions in the corrosive solution, supported by EDS and shown in Fig. 10d. Finally, figures 10e and 10g show the morphology of the steel sample surface in presence of the best organic inhibitors found in this research (compounds 5 and 7). These results suggest that the inhibitors form protective films of the surface of the API 5L X52 steel effectively diminishing corrosion. In this case, the corrosive species (Cl^-) are not observed in the chemical analysis (Figures 10f and 10h). However, as can be noted from Figure 10 in the revised version the peak associated with carbon is much intense in the presence of the inhibitor, see Figures 10f and 10h that on the bare steel sample, see Figure 10b therefore, this may be indicated of the presence of the inhibitors on the steel sample surface.

4.2 Theoretical assessment

The presence of nitrogen as heteroatom in the inhibitor molecules provides high tendency toward protonation in aqueous acidic medium. Under these conditions the calculations were carry out for the complete set of electrons and the geometry of involved structures was fully optimized. In other words, the nitrogen atoms hold positive charge by adding of hydrogen atoms and the solvent (water) effect is including with the Solvation Model based on Density (SMD) [33]. The results of the geometry optimization of the selected compounds in acidic medium and solvent effect are presented in Figure 11.

A very important fact in the adsorption over the metallic surface is the planar configuration of the inhibitor molecules. The frameworks of these geometries show no planar configurations for all the inhibitors. Some angles are showed in Figure 11, the halogen substitute has an important effect over the dihedral angle, particularly with Iodine.

Quantum-chemical indexes EHOMO, ELUMO, GAP, hardness η, and dipole moment are summarized in Table 4. It is known that EHOMO is often related to electron donation ability of the inhibitor molecules toward the metallic surface atoms, and it is expected that a higher EHOMO value would favor a greater charge transfer [70]. According to these results, the values of EHOMO show the following behavior: compound 7 > compound 6 > compound 5 > compound 3 > compound 4. In this case, the notorious largest EHOMO corresponds to compound 7 in line with the aforementioned experiments at low concentrations and the lowest EHOMO corresponds to compound 4 that in terms of activity is the worst inhibitor.

Some others authors (for instance [71]) have found that a smaller value of the hardness is related to greater stability of the surface-inhibitor complex formed. The trend that we got was 4 > 3 > 5 > 6 > 7, as it can be observed in Table 4. Then the complex metallic surface-compound 7 presents the best stability and inhibition efficiency at low concentrations.

Moreover, smaller values of ELUMO present better capacity of the inhibitor to accept electrons, for this property the trend with solvent was compound 7 < 4 < 5, 6 < 3. Negative values of ELUMO indicate the capability to accept electrons too. Nevertheless there is not a clear relationship between the above last two properties.

For the overall electrophilicity and according to the computed values (see Table 5), compound 7 exhibited a better nucleophilic character with solvent effect. Whereas compound 4 was lower than the rest. Therefore, a better interaction of compound 7 with the metallic surface would be expected than for the rest of compounds, the differences are not significant.

The Hirshfeld atomic charges for the most important centers with solvent effect are summarized in Table 6. Redistribution of the charge is observed by the presence of the substituent, the atoms that have a larger negative charge, suggests that those are active centers with excess charges that it could act as a nucleophilic group. The most favorable sites for the interaction with the metal surface are the Oxygen atoms, 24 and 25, see Figure 11 and Table 6, for all the selected compounds. As it has been expected, fluorine in compound 4 is the best electro-attractor followed by Chlorine, the halogen substitutes are active sites for the inhibition. The Carbon 8, in all the compounds, is another nucleophilic center. The Carbon 13 in compound 7 also gains charge.
Experimental data revels that compound 7 is the best inhibitor of the corrosion, the geometric structure and the parameters here studied such as EHOMO, hardness, electrophilicity and atomic charges support this fact.

5. Conclusions

The theophylline-triazole derivatives synthesized by heterogeneous catalysis were obtained in good yields. These compounds were evaluated as corrosion inhibitors in API 5L X52 steel, demonstrating that the inhibition activity of the theophylline- triazole derivatives is greater than the inhibition activities of any xanthine derivatives as theophylline, and theobromine.
The best inhibitors are the ones bearing a chlorine (compound 5) and iodine (compound 7) atoms at the para position of the aromatic ring. The best inhibition activity is reached at a concentration of 50 ppm (η of 87%). Compound 4 is the least efficient as a corrosion inhibitor, containing halogen fluoride.
These facts were confirmed by theoretical results, compound 7 exhibits a better nucleophilic character; the highest EHOMO hence underlining its good ability as an electro-donator, it has too the largest hardness with solvent effect. By another hand the worst inhibitor is the compound 4.

The adsorption study for compounds 3-7 showed that the corrosion inhibition process follows the Langmuir isotherm, with a combined physisorption-chemisorption process for compounds 3, 6 and 7. Finally, the inhibitors that carried out chemisorption process are compounds 4 and 5.
The negative values of EHOMO corroborate the physical adsorption of the inhibitors tested. The atomic charges give the sites atoms with high probability where the interaction with the metallic surface could be. In the whole set of compounds here studied, the Oxygen atoms have a large electron contribution, they can performance as electrodonating atoms. Compound 7 has one additional negative charged atom, C13.

Acknowledgments

The authors thank CONACyT for the financial support granted for the development of this research through the project P43984-Q. The authors also thank the Laboratorio de Microscopia Divisional of the Universidad Autónoma Metropolitana- Azcapotzalco for the use of the Scanning Electron Microscope SUPRA 55 VP and to the Laboratorio de Supercómputo y Visualización en Paralelo at the Universidad Autónoma Metropolitana-Iztapalapa for access to their computer facilities. AEV and FJRG express their gratitude to the Facultad de Química (UNAM), Departamento de Ingeniería Metalurgica, and CONACyT for providing a postdoctoral fellowship. AMN-L was partially supported by PRODEP program.

Competing Interests

We have no competing interests.

Authors' Contributions

Araceli Espinoza Vazquez carried out the experiments, analysis and interpretation of data by electrochemical evaluation, Deyanira Ángeles Beltran performed the surface characterization. Francisco Javier Rodríguez Gómez and Manuel Palomar Pardavé supervised all the electrochemical experiments. Guillermo E. Negrón Silva, Leticia Lomas Romero and Diego Pérez Martínez supervised the synthesis and characterization of all the triazole-theophylline compounds. Ivonne Karina Martínez Cruz was responsible for the synthesis and purification of organic compounds. Alejandra M. Navarrete-López performed the quantum chemical calculations.
All the authors gave their final approval for publication

Data availability

Our data are deposited at DRYAD DOI: https://doi.org/10.5061/dryad.k9v03g0

References

1. Machuca LL, Lepkova K and Petroski A. 2017. Corrosion of carbon steel in the presence of oilfield deposit and thiosulphate-reducing bacteria in CO_2 environment. *Corros. Sci.* **129**, 16-25.
2. Azzaoui K, Mejdoubi E, Jodeh S, Lamhamdi A, Rodriguez-Castellón E, Algarra M, Zarrouk A, Errich A, Salghi R, Lgaz H. 2017. Eco friendly green inhibitor Gum Aracbic (GA) for the corrosion control of mild steel in hydrochloric acid medium. *Corros. Sci.*, **129**, 70-81.
3. Winkier DA, Breedon M, White P, Hughes AE, Sapper ED, Cole I. 2016. Using high throughput experimental data and in silico models to discover alternatives to toxic chromate corrosion inhibitors. *Corros. Sci.*, **106** 229-235.
4. Benali O, Selles C, Salghi R. 2014. Inhibition of acid corrosion of mild steel by Anacyclus pyrethrum L. extracts. *Res. Chem. Intermed*. **40**, 259-268.
5. Karthikeyan S. 2016. Drugs/Antibiotics as potential corrosion inhibitors for Metals - A Review. *Int. J. Chem. Tech. Res*. **9**, 251-259.
6. Sanaei Z, Bahlakeh G, Ramezanzandeh B. 2017. Active corrosion protection of mild steel by an epoxy ester coating reinforced with hybrid organic/inorganic green inhibitive pigment. *J. Alloys Compd.*, **718**, 1289-1304.
7. Solmaz R, Kardaş G, Yazıcı B, Erbil M. 2008. Adsorption and corrosion inhibitive properties of 2-amino-5-mercapto-1,3,4-thiadiazole on mild steel in hydrochloric acid media. *Colloids Surf., A*, **312**, 7-17.
8. Tao Z, He W, Wang S, Zhang S, Zhou G. 2012. A study of differential polarization curves and thermodynamic properties for mild steel in acidic solution with nitrophenyltriazole derivative, *Corros. Sci.* **60**, 205-213.
9. Guo L, Qi C, Zheng X, Zhang R, Shen X, Kaya S. 2017. Toward understanding the adsorption mechanism of large size organic corrosion inhibitors on an Fe (110) surface using the DFTB method. *RSC Adv*. **7**, 29042-29050.
10. Cao Z, Tang Y, Cang H, Xu J, Lu G, Jing W. 2014. Novel benzimidazole derivatives as corrosion inhibitors of mild steel in the acidic media. Part II: Theoretical studies, *Corros. Sci.* **83**, 292-298.
11. Guo L, Obot IB, Zheng X, Shen X, Qiang Y, Kaya S, Kaya C. 2017, Theoretical insight into an empirical rule about organic corrosion inhibitors containing nitrogen, oxygen, and sulfur atoms, *Appl. Surf. Sci*. **406**, 301-306.
12. Sığırcık G, Tüken T, Erbil M. 2016. Assessment of the inhibition

efficiency of 3,4-diaminobenzonitrile against the corrosion of steel, *Corros. Sci.* **102**, 437-445.

13. Espinoza A, Negrón GE, González R., Ángeles D, Romero M, Palomar M. 2017. Effect of Hydrodynamic Conditions, Temperature and Immersion Times on the Corrosion Inhibition Efficiency of API 5L X52 Steel in 1M HCl Containing 1H-1,2,4 or 1H-1,2,3-triazoles, *Arab J. Sci. Eng*., **42**, 163-170.
14. Salarvand Z, Amirnasr M, Talebian M, Raeissi K, Meghdadi S. 2017. Enhanced corrosion resistance of mild steel in 1M HCl solution by trace amount of 2-phenyl-benzothiazole derivatives: Experimental, quantum chemical calculations and molecular dynamics (MD) simulation studies, *Corros. Sci*. **114**, 133-145.
15. Bansal R, Kumar G, Rohilla S, Klotz K. N, Kachler S, Young LC, Harvey AL. 2016. Synthesis and evaluation of a New series of 8-(2-Nitroaryl)xantines as adenosine receptor ligands. *Drug Dev. Res.* **77**, 241-250.
16. El Sayed Aly MR, Saad HA, Mosselhi M. A. 2015. Click reaction-based synthesis, antimicrobial, and cytotoxic activities of new 1,2,3-triazoles, *Med. Chem. Lett*. **25**, 2824-2830.
17. Ruddarraju RR, Murugulla AC, Kotla R, Tirumalasetty MCB, Wudayagiri R, Donthabakthuni S, Maroju R. 2017. Design, synthesis, anticancer activity and docking studies of theophylline containing 1,2,3-triazoles with variant amide derivatives. *Med. Chem. Commun.* **8**, 176-183.
18. Soltani MN, Behrouz S, Najafi H. 2014. N-Tosyltheophylline (TsTh): A highly Efficient reagent for the one-pot synthesis of N-alkyltheophyllines from alcohols. *Synthesis*, **46**, 1380-1388.
19. Andrs M, Muthna D, Rezacova M, Seifrtova M, Siman P, Korabecny J, Benek O, Dolezal R, Soukup O, Jun D, Kuca K. 2016. Novel caffeine derivatives with antiproliferative activity. *RSC Adv.* **6**, 32534-32539.
20. Hayallah AM, Elgaher WA, Salem O. I, Abdel AAM. 2011. Design and synthesis of some new theophylline derivatives with bronchodilator and antibacterial activities. *Arch. Pharm. Res.* **34**, 3-21.
21. Ruddarraju RR, Murugulla AC, Kotla R, Tirumalasetty MCB, Wudayagiri R, Donthabakthuni S, Maroju R, Baburao K, Parasa LS. 2016. Design, synthesis, anticancer, antimicrobial activities and molecular docking studies of theophylline containing acetylenes and theophylline containing 1,2,3-triazoles with variant nucleoside derivatives, *Eur. J. Med. Chem.* **123**, 379-396.
22. Cuong NT, Tai TB, Thu Ha VT, Nguyen M. T. 2010. Thermochemical parameters of caffeine, theophylline and xanthine. *J. Chem. Thermodyn*., **42**, 437-440.
23. De Souza FS, Giacomelli C, Gonçalves RS, Spinelli A. 2012. Assessment of caffeine adsorption onto mild steel surface as an eco-friendly corrosion inhibitor, *Mater. Sci. Eng. C Mater. Biol. Appl*. **32**, 2436.
24. Espinoza A, Rodríguez FJ, Martínez IK, Negrón GE, Palomar M. 2018. Determination of Inhibition Properties of Caffeine, Theophylline and their Allylic and Propargylic Derivatives on API 5L X70 Steel Immerse in 1M HCl. *ECS transactions*, **84**(1) 165-171.
25. Ma Q, Qi S, He X, Tanga Y, Lub G. 2017. 1,2,3-Triazole derivatives as corrosion inhibitors for mild steel in acidic medium: Experimental and computational chemistry studies, *Corros. Sci*. **129**, 91-101.
26. AL Jahdaly BA, Awad MI. 2016. Enhanced inhibition of corrosión of mild Steel by triazole derivative in presence of copper ions. *Int. J. Electrochem. Sci.* **11**, 5473-5480.
27. Ofoegbu SU, Galvão TLP, Gomes J. RB, Tedim J, Nogueira HIS, Ferreira MGS, Zheludkevich ML. 2017. Corrosion inhibition of copper in aqueous chloride solution by 1*H*-1,2,3-triazole and 1,2,4-triazole and their combinations: electrochemical, Raman and theoretical studies, *Phys. Chem. Chem. Phys.* **19**, 6113-6129.
28. Yan Y, Lin X, Zhang L, Zhou H, Wu L, Cai L. 2017. Electrochemical and quantum-chemical study on newly synthesized triazoles as corrosion inhibitors of mild steel in 1 M HCl, *Res. Chem. Intermed*. **43,** 3145-3154.
29. Espinoza A, Rodríguez FJ, Vergara BI, Lomas L, Ángeles D, Negrón GE, Morales JA. 2017. Synthesis of 1,2,3-triazoles in the presence of mixed Mg/Fe oxides and their evaluation as corrosion inhibitors of API 5L X70 steel submerged in HCl, *RSC Adv.* **7**, 24736-24746.
30. González R, Román V, Negrón GE, Espinoza A, Rodríguez FJ, Santillán R. 2016. Multicomponent Synthesis and Evaluation of New 1,2,3-Triazole Derivatives of Dihydropyrimidinones as Acidic Corrosion Inhibitors for Steel, *Molecules*, **21**, 250-3-13.
31. Espinoza A, Negrón GE, González R, Ángeles D, Herrera H, Romero M, Palomar M. 2014. Mild steel corrosion inhibition in HCl by di-alkyl and di-1,2,3-triazole derivatives of uracil and Thymine. *Mater. Chem. Phys.,* **145**, 407-417.
32. Espinoza A, Rodríguez FJ, González R, Ángeles D, Mendoza D, Negrón G E, 2016. Electrochemical assessment of phenol and triazoles derived from phenol (BPT) on API 5L X52 steel immersed in 1 M HCl. RSC *Adv*., **6**, 72885-72896.
33. Frisch MJ, Trucks GW, Schlegel HB, Scuseria GE, Robb MA, Cheeseman JR, Scalmani G, Barone V, Mennucci B, Petersson GA, Nakatsuji H, Caricato M, Li X, Hratchian HP, Izmaylov AF, Bloino J, Zheng G, Sonnenberg JL, Hada M, Ehara M, Toyota K, Fukuda R, Hasegawa J, Ishida M, Nakajima T, Honda Y, Kitao O, Nakai H, Vreven T, Montgomery JrJA, Peralta JE, Ogliaro F, Bearpark M, Heyd JJ, Brothers E, Kudin KN, Staroverov VN, Kobayashi R, Normand J, Raghavachari K, Rendell A, Burant JC, Iyengar SS, Tomasi J, Cossi M, Rega N, Millam JM, Klene M, Knox JE, Cross JB, Bakken V, Adamo C, Jaramillo J, Gomperts R, Stratmann RE, Yazyev O, Austin AJ, Cammi R, Pomelli C, Ochterski JW, Martin RL, Morokuma K, Zakrzewski VG, Voth GA, Salvador P, Dannenberg JJ, Dapprich S, Daniels AD, Farkas Ö, Foresman JB, Ortiz JV, Cioslowski J, Fox DJ. 2009. Gaussian 09 (Gaussian, Inc., Wallingford CT).
34. Zhao Y, Truhlar DG. 2008. The M06 Suite of Density Functionals for main group thermochemistry, thermochemical kinetics, noncovalent Interactions, excited states, and transition elements: two new functionals and systematic testing of four M06- class functionals and 12 other functionals. Theor. Chem. Acc., **120**, 215-241.
35. Marenich AV, Cramer CJ, Truhlar DG. 2009. Universal solvation model based on solute electron density and a continuum model of the solvent defined by the bulk dielectric constant and atomic surface tensions. J. Phys. Chem. B, **113**, 6378-6396.
36. Obayes HR, Al-Amiery AA, Alwan G H, Amir A, Kadhum H, Mohamad A B. 2017. Sulphonamides as corrosion inhibitor: Experimental and DFT studies. *J. of Mol. Struct*. 1138, 27-34
37. Obot IB, Ankah NK, Sorour AA, Gasem ZM, Haruna K. 2017. 8-Hydroxyquinoline as an alternative green and sustainable acidizing oilfield corrosion inhibitor. *Sust. Mat. and Techn*., **14**, 1-10
38. Pfeiffer M, Klock H, Helmut, Bergen G. Ehrenhaft, Ferreira P, Gollnick J., Fischer CB. 2017. Surface protection of low carbon steel with N-acyl

sarcosine derivatives as green corrosion inhibitors. *Surf. Interfaces*, **9**, 70-78.

39. Qiang Y, Zhang S, Yan S, Zou X, Chen S. 2017. Three indazole derivatives as corrosion inhibitors of copper in a neutral chloride solution. *Corros. Sci*. **126**, 295-304.
40. Yadav M, Behera D, Sharma U. 2016. Nontoxic corrosion inhibitors for N80 steel in hydrochloric acid. *Arab. J. of Chem*., **9**(2), s1487-s1495.
41. Mobin M, Basik M, Aslam J. 2018. Boswellia serrata gum as highly efficient and sustainable corrosion inhibitor for low carbon steel in 1 M HCl solution: Experimental and DFT studies. *J. Mol. Liq*. **263**, 174–186
42. Javadian S, Yousefi A, Neshati J. 2013. Synergistic effect of mixed cationic and anionic surfactants on the corrosion inhibitor behavior of mild steel in 3.5% NaCl. *Appl. Surf. Sci*. **285**, 674–681.
43. Zarrouk A, Zarrok H, Ramli Y. 2016. Inhibitive properties, adsorption and theoretical study of 3,7-dimethyl-1-(prop-2-yn-1-yl)quinoxalin-2(1H)-one as efficient corrosion inhibitor for carbon steel in hydrochloric acid solution. *J. Mol. Liq*. **222**, 239–252.
44. Mo S, Jie L, Qun H, Bing N. 2017. An example of green copper corrosion inhibitors derived from flavor and medicine: Vanillin and isoniazid. *J. of Mol. Liq*. **242**, 822-830
45. Zeino A, Abdulazeez I, Khaled M, Jawich MW, Obot IB. 2018. Mechanistic study of polyaspartic acid (PASP) as eco-friendly corrosion inhibitor on mild steel in 3% NaCl aerated solution. *J. of Mol. Liq*., **250**, 50-62.
46. Ebenso EE, Kabanda MM. 2012. Electrochemical and quantum chemical investigation of some azine and thiazine dyes as,potential corrosion inhibitors for mild steel in hydrochloric acid solution. *Ind. Eng. Chem. Res*. **51**, 12940–12958.
47. Zhang H, Pang X, Zhou M, Liu C, Wei L, Gao K. 2015. The behavior of pre-corrosion effect on the performance of imidazoline-based inhibitor in 3 wt.% NaCl solution saturated with CO_2, *Appl. Surf. Sci.* **356**: 63–72.
48. Singh D, Ansari KR, Sorour AA, Quraishi MA., Gaz HL, Salghi R. 2018. Thiosemicarbazide and thiocarbohydrazide functionalized chitosan as ecofriendly corrosion inhibitors for carbon steel in hydrochloric acid solution, *Int. J. of Biol. Macrom*. **107**, 1747-1757.
49. Kadhim A, Al-Okbi AK, Jamil DM, Qussay A, Al-Amiery AA, Sumer T, Kadhum AAH, Mohamad AB, Nassir MH. 2017. Experimental and theoretical studies of benzoxazines corrosion inhibitors, *Results in Phys*. **7**, 4013-4019.
50. Chidiebere MA, Oguzie EE, Liu L, Li Y, Wang F. 2015. Adsorption and corrosion inhibiting effect of riboflavin on Q235 mild steel corrosion in acidic environments, *Mat. Chem. and Phys.* **156**, 95-104.
51. Prabakaran M, HyunKim S, Mugila N, Hemapriya V, Parameswari K, Chitra S. 2017. Aster koraiensis as nontoxic corrosion inhibitor for mild steel in sulfuric acid, J. of Ind. and Eng. Chem. **52**, 235-242.
52. Ansari KR, Quraishi MA, Singh A. 2017. Chromenopyridin derivatives as environmentally benign corrosion inhibitors for N80 steel in 15% HCl, *J. of the Assoc. of Arab Universit. for Basic and Appl. Sci*. **22**, 45-54.
53. Hamani H, Douadi T, Daoud D, Al-Noaimi M, Amina R, Chafaa S. 2017. 1-(4-Nitrophenylo-imino)-1-(phenylhydrazono)-propan-2-one as corrosion inhibitor for mild steel in 1M HCl solution: Weight loss, electrochemical, thermodynamic and quantum chemical studies. *J. of Electroanal. Chem*. **801**, 425-438.
54. Bedair MA, El-Sabbah MMB, Fouda AS, Elaryian HM. 2017. Synthesis, electrochemical and quantum chemical studies of some prepared surfactants based on azodye and Schiff base as corrosion inhibitors for steel in acid medium, *Corros. Sci.* **128**, 54-72.
55. Quraishia MA, Lgazd H, Salghi R. 2018. Thiosemicarbazide and thiocarbohydrazide functionalized chitosan as ecofriendly corrosion inhibitors for carbon steel in hydrochloric acid solution, *Int. J. Biol. Macrom.,* **107**, 1747–1757.
56. Stoyanova A, Petkova G, Peyerimhoff S. 2002. Correlation between the molecular structure and the corrosion inhibiting effect of some pyrophthalone compounds, *Chem. Phys.* **279** (1), 1–6.
57. Solmaz R, Kardas G, Culha M, Yazıcı B, Erbil M, 2008. Investigation of adsorptionand inhibitive effect of 2-mercaptothiazoline on corrosion of mild steel inhydrochloric acid media, *Electrochim. Acta* **53** (20), 5941–5952.
58. Lee H, Abdul A, Yuen C, Saad B, Idris M, Umeda M. 2017. Aquilaria subintergra leaves extracts as sustainable mild steel corrosion inhibitors in HCl. *Meas.* 109, 334-345.
59. Shihab MS, Al-Doori HH. 2014. Experimental and theoretical study of [N-substituted] p-aminoazobenzene derivatives as corrosion inhibitors for mild steel in sulfuric acid solution, *J. of Mol. Struct*. **1076**, 658-663.
60. Singh P, Quraishi MA. 2016. Corrosion inhibition of mild steel using Novel Bis Schiff's Bases as corrosion inhibitors: Electrochemical and Surface measurement. *Meas*., **86**, 114-124.
61. Hu K, Zhuang J, Zheng C, Ma Z, Ding J. 2016. Effect of novel cytosine-l-alanine derivative based corrosion inhibitor on steel surface in acidic solution. *J. of Mol. Liq*. **222**, 109-117.
62. Hu Z, Bin Y, Ma X, Zhu H, Li J, Li C, Lin D. 2016, Experimental and theoretical studies of benzothiazole derivatives as corrosion inhibitors for carbon steel in 1M HCl, *Corros. Sci*., **112**, 563-575.
63. Mobin M, Rizvi M. 2017. Polysaccharide from Plantago as a green corrosion inhibitor for carbon steel in 1M HCl solution. *Carbohydr. Polym.* **160**, 172-183.
64. Ostapenko GI, Gloukhov PA, Bunev AS, 2014. Investigation of 2-cyclohexenylcyclohexanone as steel corrosion inhibitor and surfactant in hydrochloric acid. *Corros. Sci*., **82**, 265-270.
65. Anupama KK, Ramya K, Shainy KM, Joseph A, 2015. Adsorption and electrochemical studies of Pimenta dioica leaf extracts as corrosion inhibitor for mild steel in hydrochloric acid, *Mat. Chem. and Phys*. **167**, 28-41.
66. Lokov M, Tshepelevitsh S, Heering A, Plieger PG, Vianello R, and Leit I. 2017, On the Basicity of Conjugated Nitrogen Heterocycles in Different Media, *Eur. J. Org. Chem*. 4475–4489
67. Hamania H, Douadia T, Daouda D, Al-Noaimic M, Rikkouha R, Chafaa S. 2017. 1-(4-Nitrophenylo-imino)-1-(phenylhydrazono)-propan-2-one as corrosion inhibitor for mild steel in 1 M HCl solution: Weight loss, electrochemical, thermodynamic and quantum chemical studies, *J. Electroanalyt. Chem.* **801**, 425–438.
68. Singh P, Quraishi MA. 2016. Corrosion inhibition of mild steel using Novel Bis Schiff's Bases as corrosion inhibitors: Electrochemical and Surface. *Measurement* **86**, 114–124.
69. Haldhar R, Prasad D, Saxena A. 2018. Myristica fragrans extract as an eco-friendly corrosion inhibitor for mild steel in 0.5 M H_2SO_4 solution*, J. Environm. Chem. Eng.* **6**, 2290–2301.
70. Khaled KF. 2008. Molecular simulation, quantum chemical calculations and electrochemical studies for inhibition of mild Steel by triazoles. *Electrochim. Acta*, **53**, 3484-3492.

71. Sahin M, Gece G, Kaerci F, Bligic S. Experimental and theoretical study of the effect of some heterocyclic compounds on the corrosión of low carbon steel in 3.5% NaCl medium. *J. Appl. Electrochem.*, **38**, 809-815.

Tables

Table 1. *Electrochemical parameters of 1,2,3-triazoles 1,4-disubstituted in API 5L X52 steel immerse in HCl 1M*

Inhibitor	C (ppm)	Rs (Ω cm^2)	n	C_{dl} (μF cm^{-2})	R_{ct} (Ω cm^2)	R_{mol} (Ω cm^2)	η (%)	Chi squared
blank	0	0.8	0.8	310.0	30	-	-	-
	5	1.1	0.72	221.9	154.0	5.1	81.1	0.0833
3	10	1.2	0.69	230.7	227.6	13.4	87.6	0.1119
	20	1.0	0.67	205.1	286.1	16.2	90.1	0.1130
	50	1.1	0.68	195.4	343.1	17.3	91.7	0.1052
	5	1.1	0.73	228.9	49.9	9.6	49.6	0.1447
	10	1.3	0.75	192.8	112.4	18.9	77.2	0.1672
4	20	1.2	0.72	193.4	168.1	19.5	84.0	0.1415
	50	1.2	0.71	182.7	210.4	18.6	86.9	0.1366
	5	11.5	0.74	247.3	35.4	36.8	58.4	0.0020
5	10	8.0	0.88	214.8	68.1	16.7	64.6	0.0016
	20	8.5	0.95	170.8	265.7	5.4	88.9	0.0017
	50	6.3	0.62	89.9	492.8	6.7	94.0	0.0014
	5	1.0	0.70	174.4	134.5	14.4	79.9	0.1245
6	10	1.1	0.72	129.4	169.8	29.8	85.0	0.0893
	20	1.1	0.68	123.2	248.4	28.7	89.2	0.1065
	50	1.2	0.63	108.2	335.3	29.5	91.8	0.1065
	5	1.5	0.70	172.7	201.8	5.1	85.5	0.0024
7	10	1.0	0.65	153.4	224.1	0.5	86.6	0.0036
	20	0.9	0.63	158.1	272.4	2.6	89.1	0.0045
	50	1.0	0.60	153.2	328.2	2.9	90.9	0.0040

Table 2. *Electrochemical parameters obtained by means of polarization curves for 1,2,3-triazoles 1,4-disubstited in API 5L X52 steel immerse in HCl 1M*

Inhibitor	C (ppm)	Ecorr (mV) vs Ag/AgCl	bc (mV dec-1)	ba (mV dec-1)	icorr (mA/cm2)	ηpol (%)
BLANK	0	-421.2	-106.5	84.6	0.32	-
3	5	-450.8	-107.0	54.3	0.04	87.3
3	50	-470.1	-109.5	75.0	0.04	86.9
4	5	-448.0	-163.4	80.4	0.08	76.6
4	50	-439.9	-158.8	74.7	0.04	87.0
5	5	-447.6	-146.8	52.6	0.07	79.4
5	50	-441.0	-110.2	66.3	0.02	71.0
6	5	-413.4	-122.1	30.5	0.02	94.3
6	50	-427.2	-136.2	48.4	0.02	93.5
7	5	-410.8	-161.2	52.1	0.03	90.3
7	50	-425.3	-132.2	69.5	0.04	88.2

***Table 3**. Adjustment of thermodynamic data with the Langmuir isotherm*

Compound	Kads	ΔG° ads (kJ mol^{-1})	Slopes (M)	R^2
3	2.66 x 10^7	-41.7	C / θ =1.0.759C	0.9982
4	5.95 x 10^6	-38.1	C / θ =1.0788C	0.9979
5	5.38 x 10^6	-37.8	C / θ =0.9749C	0.9965
6	2.66 x10^7	-41.7	C / θ =1.0700C	0.9998
7	5.37 x10^7	-43.4	C / θ =1.0895C	0.9989

***Table 4.** Values for EHOMO, ELUMO, GAP, global hardness (η) for the inhibitors (in vacuo/with solvent) and total energy stabilization by solvent effect (ΔEsolv).*

Compound	EHOMO (eV)	ELUMO (eV)	GAP (eV)	η (eV)	ΔEsolv (eV)
3	-13.45/-8.60	-8.18/-1.26	5.27/7.34	2.64/3.67	-8.41
4	-13.73/-8.69	-8.25/-1.29	5.48/7.41	2.74/3.70	-8.63
5	-13.22/-8.53	-8.24/-1.28	4.98/7.25	2.49/3.63	-8.61
6	-12.61/-8.32	-8.22/-1.28	4.39/7.04	2.20/3.52	-8.57
7	-11.99/-7.75	-8.19/-1.32	3.79/6.43	1.90/3.22	-8.53

***Table 5.** Values for chemical potential and electrophilicity (in vacuo/with solvent)*

Compound	Chemical Potential (μ) (eV)	Electrophilicity (W) (eV)
3	-10.81/-4.93	22.17/3.31
4	-10.99/-4.99	22.03/3.36
5	-10.73/-4.90	23.10/3.32
6	-10.41/-4.80	24.68/3.27
7	-10.09/-4.54	26.85/3.20

Table 6. Atomic Hirshfeld charges for the different inhibitor compounds. See the Figure 11 for the atomic labels.

Number	Atom	Compound 3	Compound 4	Compound 5	Compound 6	Compound 7
1	N	-0.011	-0.005	-0.007	-0.011	-0.003
2	N	0.305	0.306	0.306	0.310	0.313
3	N	0.087	0.088	0.087	0.087	0.090
4	C	0.164	0.178	0.177	0.151	0.188
5	C	0.074	0.075	0.074	0.075	0.077
6	C	0.275	0.275	0.276	0.274	0.276
7	C	0.210	0.218	0.219	0.216	0.227
8	C	-0.020	-0.019	-0.015	-0.012	-0.013
9	C	0.020	0.040	0.041	0.044	0.036
10	C	0.027	0.048	0.048	0.050	0.001
11	C	0.015	0.026	0.024	0.013	0.029
12	C	0.015	0.026	0.023	0.012	0.027
13	C	0.017	0.094	0.036	-0.004	-0.031
14	**H**	**0.000**	**-0.167**	**-0.110**	**-0.038**	**-0.038**
15	N	0.025	0.024	0.025	0.025	0.025
16	C	0.358	0.358	0.359	0.356	0.358
17	N	0.245	0.245	0.245	0.245	0.245
18	C	0.165	0.165	0.165	0.165	0.166
19	C	0.015	0.015	0.014	0.015	0.015
20	N	0.165	0.165	0.165	0.165	0.165
21	C	0.213	0.213	0.212	0.215	0.213
22	N	0.127	0.127	0.127	0.127	0.127
23	C	0.271	0.271	0.271	0.270	0.271
24	O	-0.353	-0.354	-0.352	-0.343	-0.352
25	O	-0.411	-0.411	-0.410	-0.411	-0.411

Figure and table captions

Figure 1 Synthesis of 1,2,3-triazoles in presence of Cu(Al)O.

Figure 2 Equivalent electric circuit used in the system with (b) and without inhibitor (a).

Figure 3 a) Open Circuit Potential (OCP) vs time of theophylline-triazoles derivatives at 50 ppm and b) Nyquist diagram without inhibitor in immerse API 5L X52 steel.

Figure 4 Nyquist diagrams of theophylline-triazoles in immerse API 5L X52 steel at different inhibitor concentrations. Diagrams a), b), c), d) and e) corresponds to compounds 3, 4, 5, 6 and 7 respectively.

Figure 5 Bode diagrams of theophylline-triazoles compounds: a) 3, b) 4, c) 5, d) 6 and e) 7 immersed API 5L X52 steel at different inhibitor concentrations.

Figure 6 Variation of the inhibition efficiency of the theophylline-triazole derivatives 3-7 as a function of its concentration for API 5L X70 steel submerged in 1 M HCl by EIS technique.

Figure 7 Potentiodynamic polarization curves of 1,2,3-triazoles 1,4-disubstituted in API 5L X52 steel immerse in 1M of HCl.

Figure 8 Adjustment of the thermodynamic analysis of the theophylline-triazole derivatives by using a) Langmuir model and b) in API 5L X52 steel immerse in HCl 1M.

Figure 9 Schematic representation of the adsorption behavior of inhibitor on API 5L X52 steel surface immersed in 1M HCl.

Figure 10. Images of SEM-EDS of API 5L X52 steel for a) polished steel, c) immerse in HCl 1M and in presence of 50 ppm of e) compound 5 and g) compound 7.

Figure 11. Optimized molecular structures: (a) compound 3, (b) compound 4, (c) compound 5, (d) compound 6, (e) compound 7. Carbon atoms are represented in gray ball, Nitrogen in dark blue, Oxygen in red and Hydrogen in white color. Dihedral angle among 3,7,8 and 10 atoms.

FIGURE 1

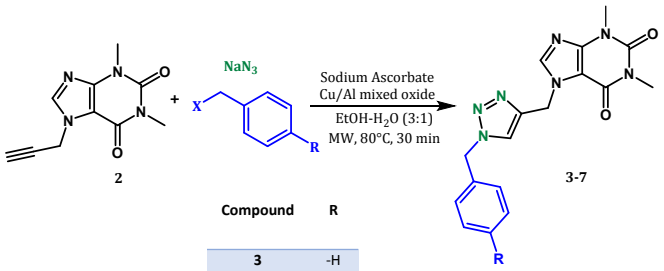

Compound	R
3	-H
4	-F
5	-Cl
6	-Br
7	-I

a)

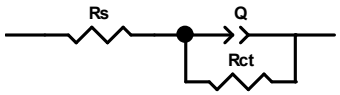

b)

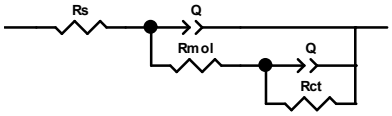

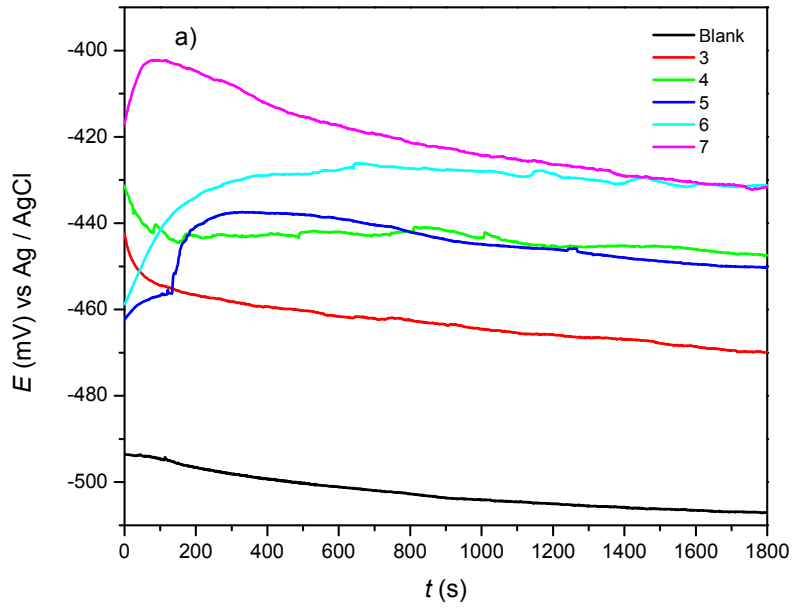
a)
Blank
3
4
5
6
7
E (mV) vs Ag / AgCl
t (s)
-400
-420
-440
-460
-480
-500
0
200
400
600
800
1000
1200
1400
1600
1800

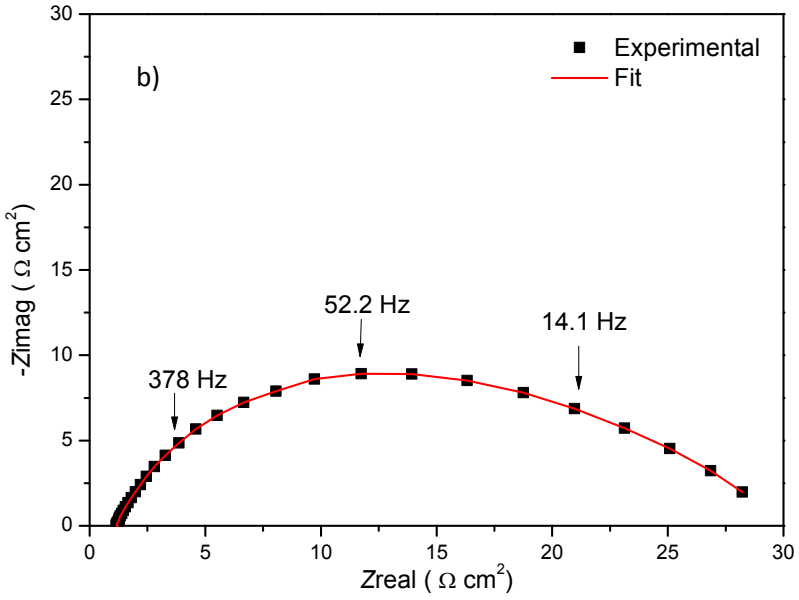
b)
Experimental
Fit
52.2 Hz
14.1 Hz
378 Hz
-Zimag (Ω cm2)
Zreal (Ω cm2)
0
5
10
15
20
25
30

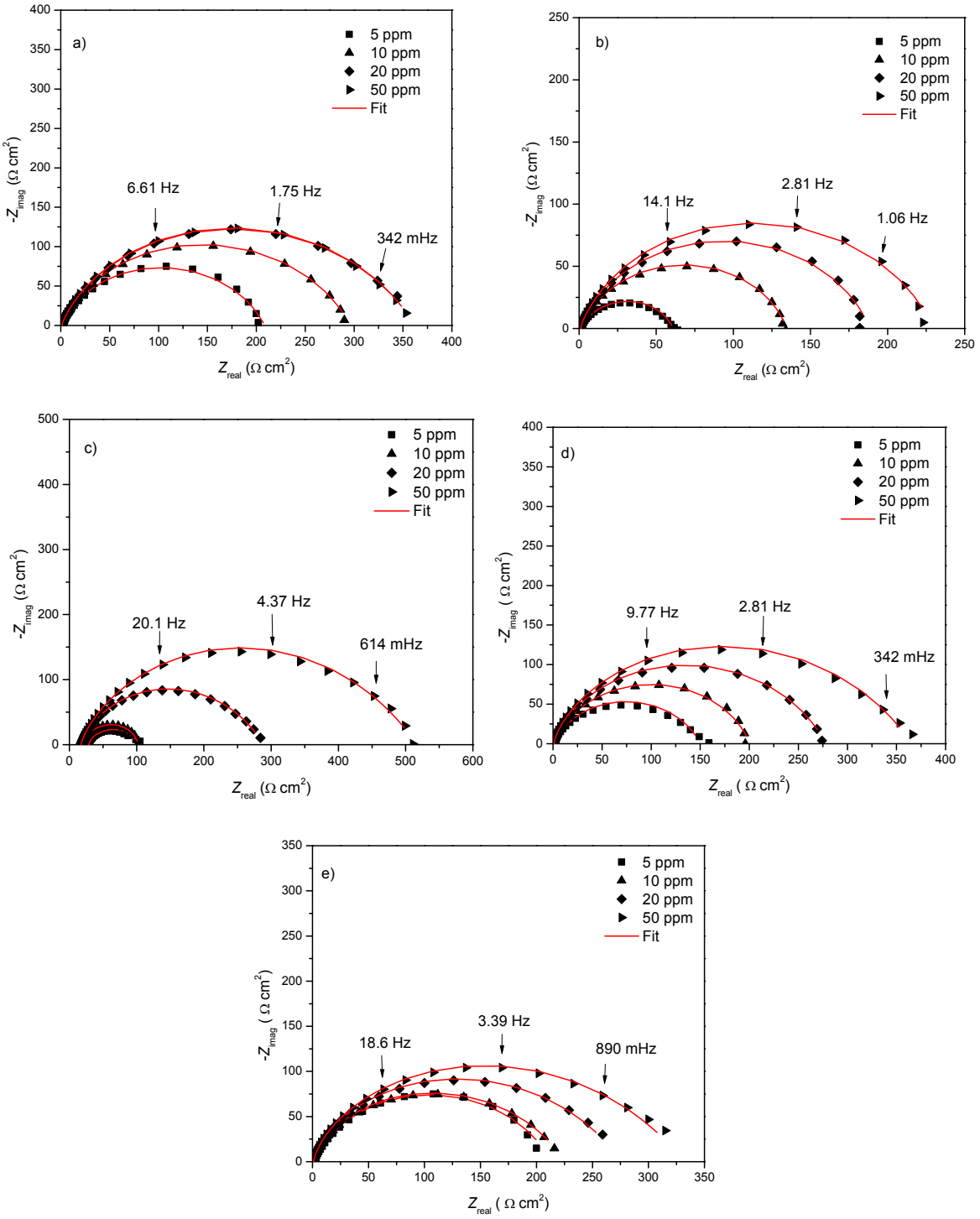
a)
5 ppm
10 ppm
20 ppm
50 ppm
Fit
6.61 Hz
1.75 Hz
342 mHz
$-Z_{imag}$ (Ω cm^2)
Z_{real} (Ω cm^2)
b)
5 ppm
10 ppm
20 ppm
50 ppm
Fit
14.1 Hz
2.81 Hz
1.06 Hz
$-Z_{imag}$ (Ω cm^2)
Z_{real} (Ω cm^2)
c)
5 ppm
10 ppm
20 ppm
50 ppm
Fit
20.1 Hz
4.37 Hz
614 mHz
$-Z_{imag}$ (Ω cm^2)
Z_{real} (Ω cm^2)
d)
5 ppm
10 ppm
20 ppm
50 ppm
Fit
9.77 Hz
2.81 Hz
342 mHz
$-Z_{imag}$ (Ω cm^2)
Z_{real} (Ω cm^2)
e)
5 ppm
10 ppm
20 ppm
50 ppm
Fit
18.6 Hz
3.39 Hz
890 mHz
$-Z_{imag}$ (Ω cm^2)
Z_{real} (Ω cm^2)

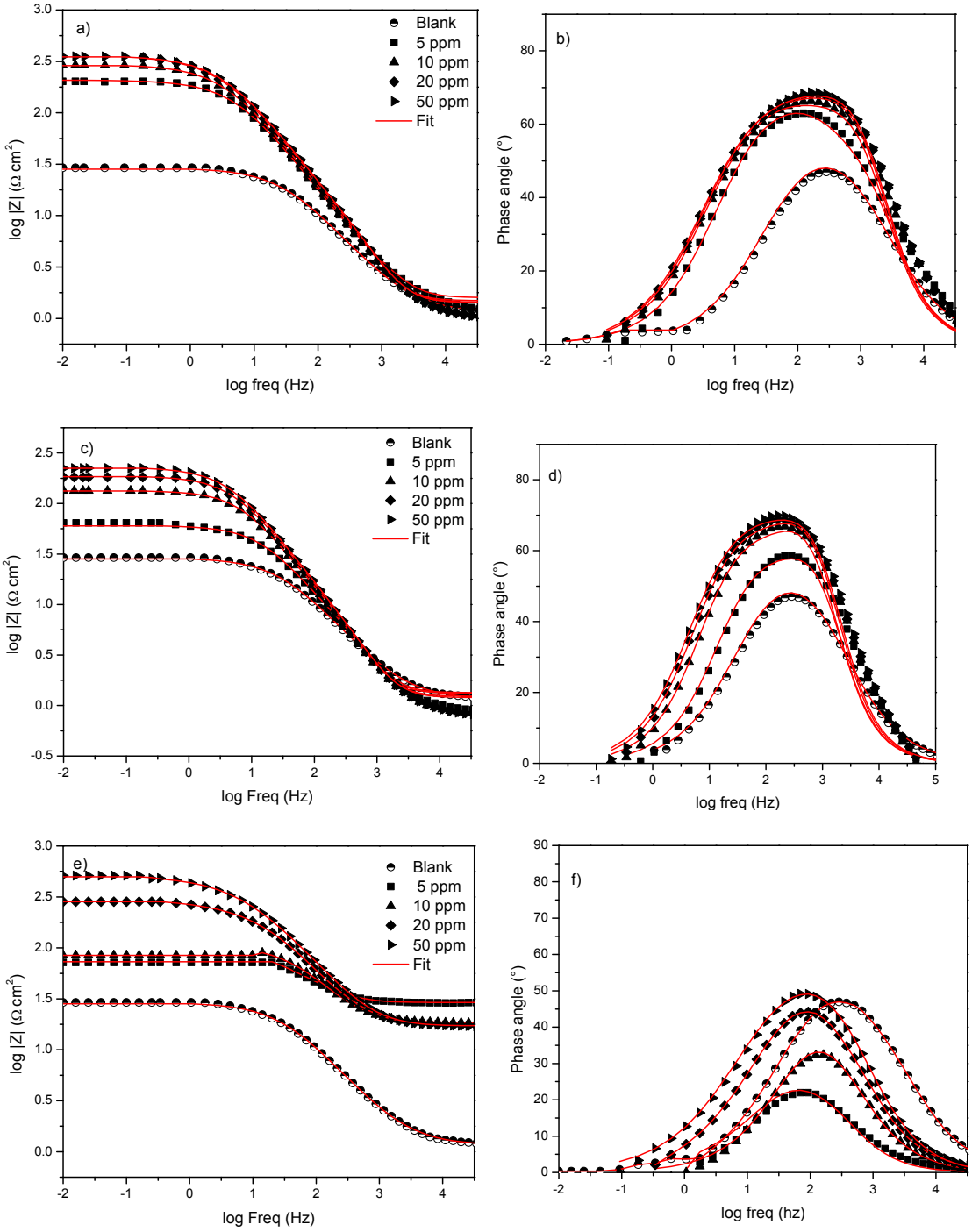
a)
Blank
5 ppm
10 ppm
20 ppm
50 ppm
Fit
log |Z| (Ω cm²)
log freq (Hz)
b)
Phase angle (°)
log freq (Hz)
c)
Blank
5 ppm
10 ppm
20 ppm
50 ppm
Fit
log |Z| (Ω cm²)
log Freq (Hz)
d)
Phase angle (°)
log freq (Hz)
e)
Blank
5 ppm
10 ppm
20 ppm
50 ppm
Fit
log |Z| (Ω cm²)
log Freq (Hz)
f)
Phase angle (°)
log freq (hz)

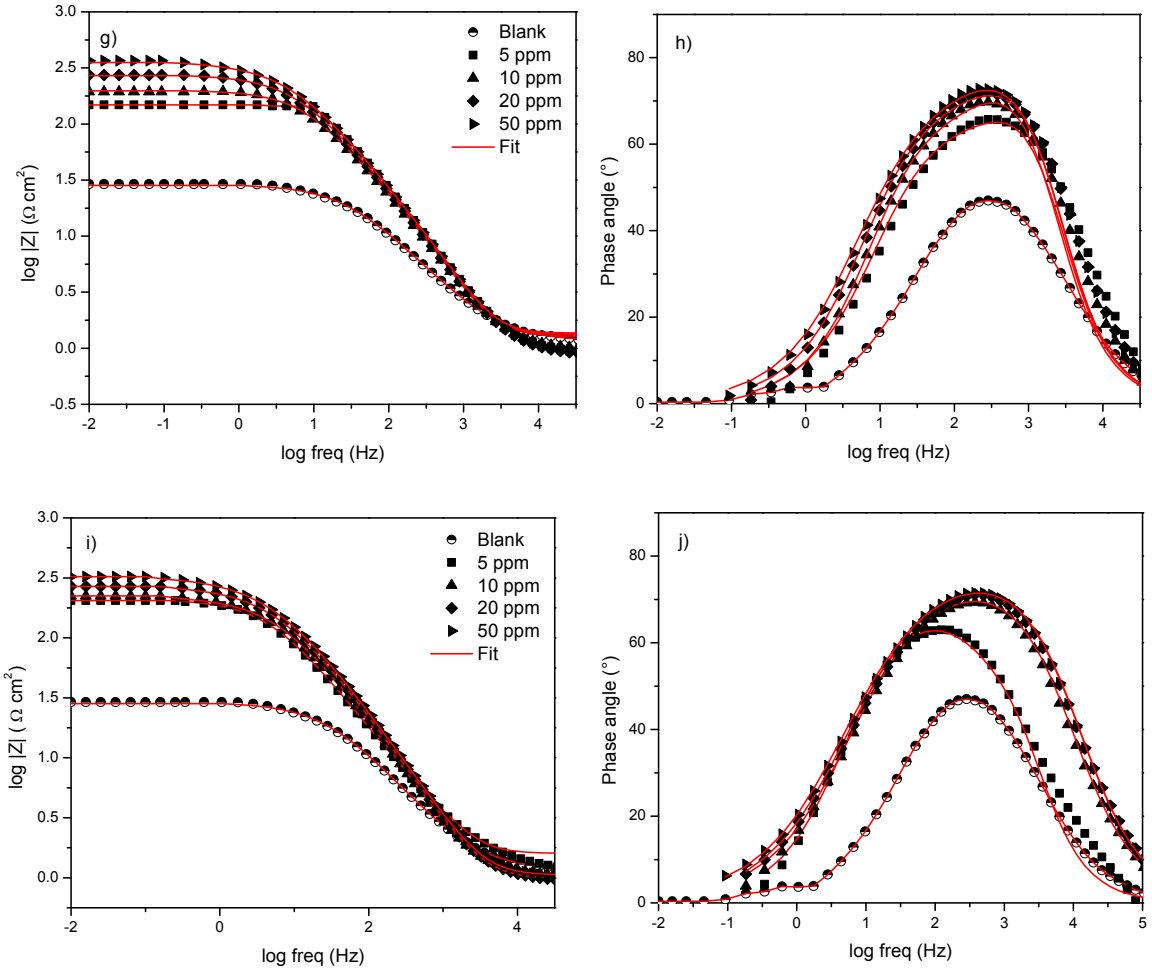
g)
Blank
5 ppm
10 ppm
20 ppm
50 ppm
Fit
log |Z| (Ω cm²)
log freq (Hz)
h)
Phase angle (°)
log freq (Hz)
i)
Blank
5 ppm
10 ppm
20 ppm
50 ppm
Fit
log |Z| (Ω cm²)
log freq (Hz)
j)
Phase angle (°)
log freq (Hz)

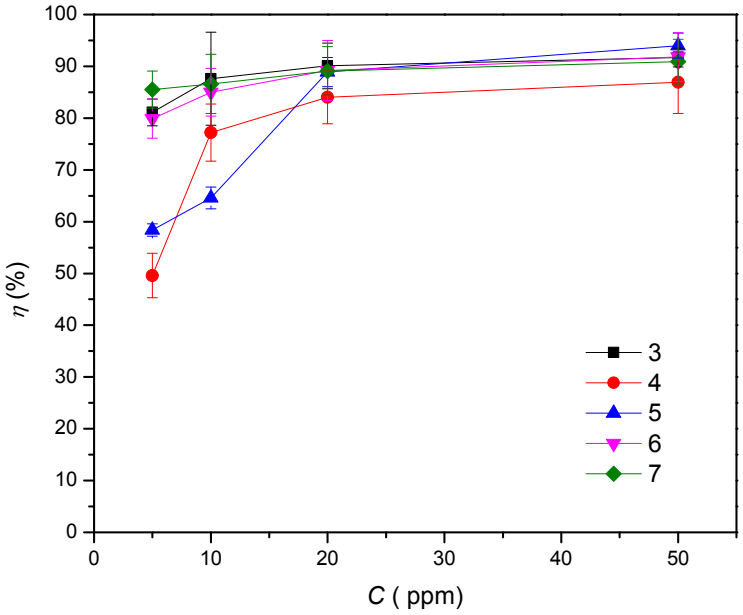
100
90
80
70
60
50
40
30
20
10
0
η (%)
0
10
20
30
40
50
C (ppm)
3
4
5
6
7

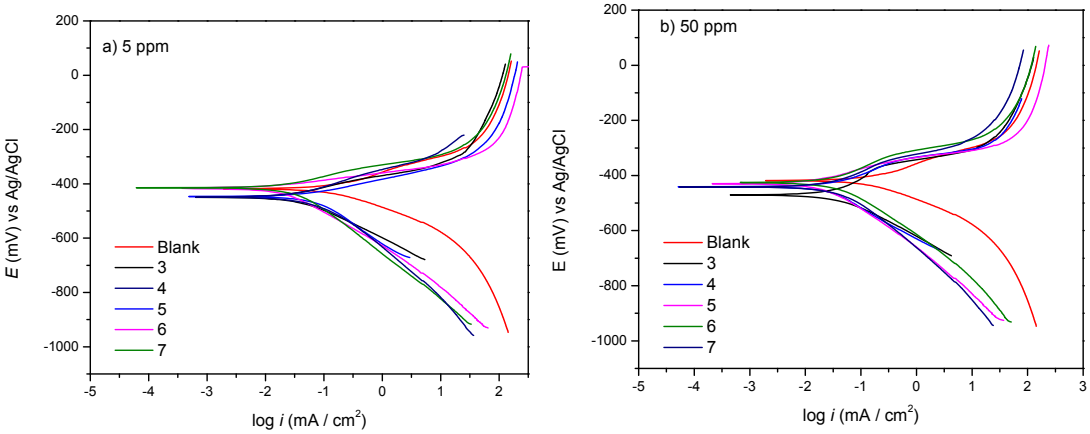
a) 5 ppm
E (mV) vs Ag/AgCl
log i (mA / cm2)
Blank
3
4
5
6
7
b) 50 ppm
E (mV) vs Ag/AgCl
log i (mA / cm2)
Blank
3
4
5
6
7

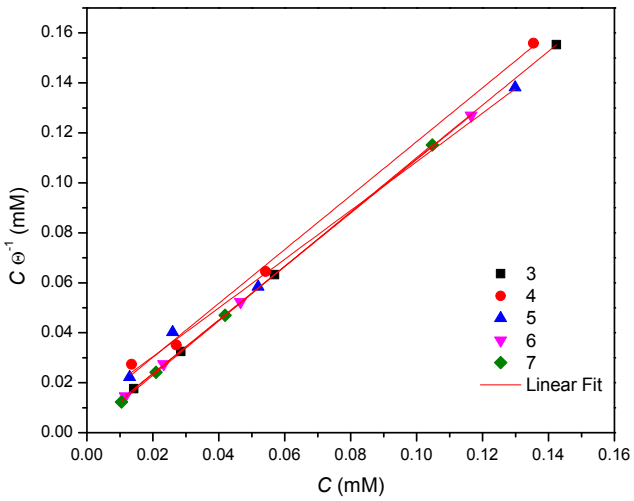
0.16
0.14
0.12
0.10
0.08
0.06
0.04
0.02
0.00
C Θ-1 (mM)
0.00
0.02
0.04
0.06
0.08
0.10
0.12
0.14
0.16
C (mM)
3
4
5
6
7
Linear Fit

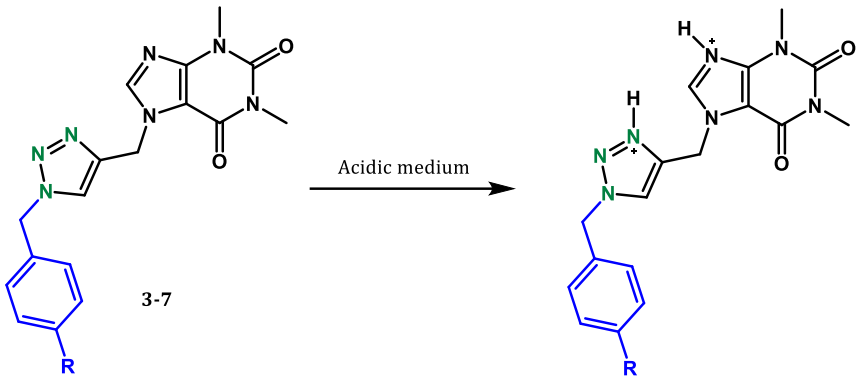

Compound	R
3	-H
4	-F
5	-Cl
6	-Br
7	-I

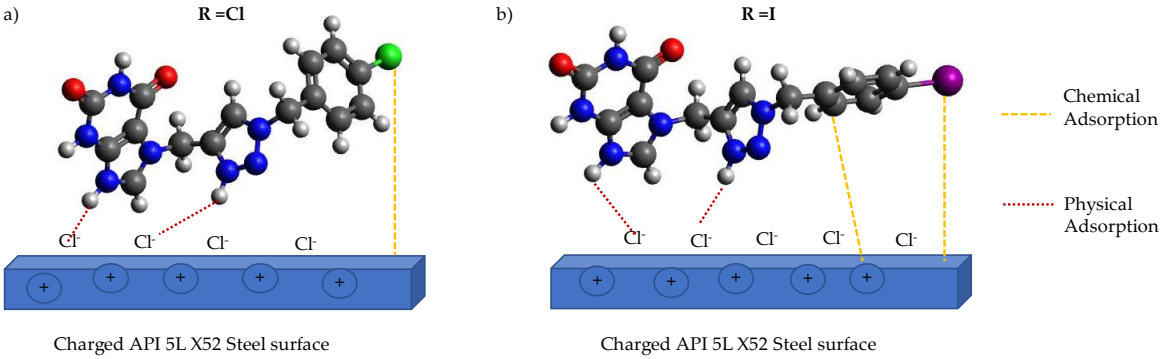

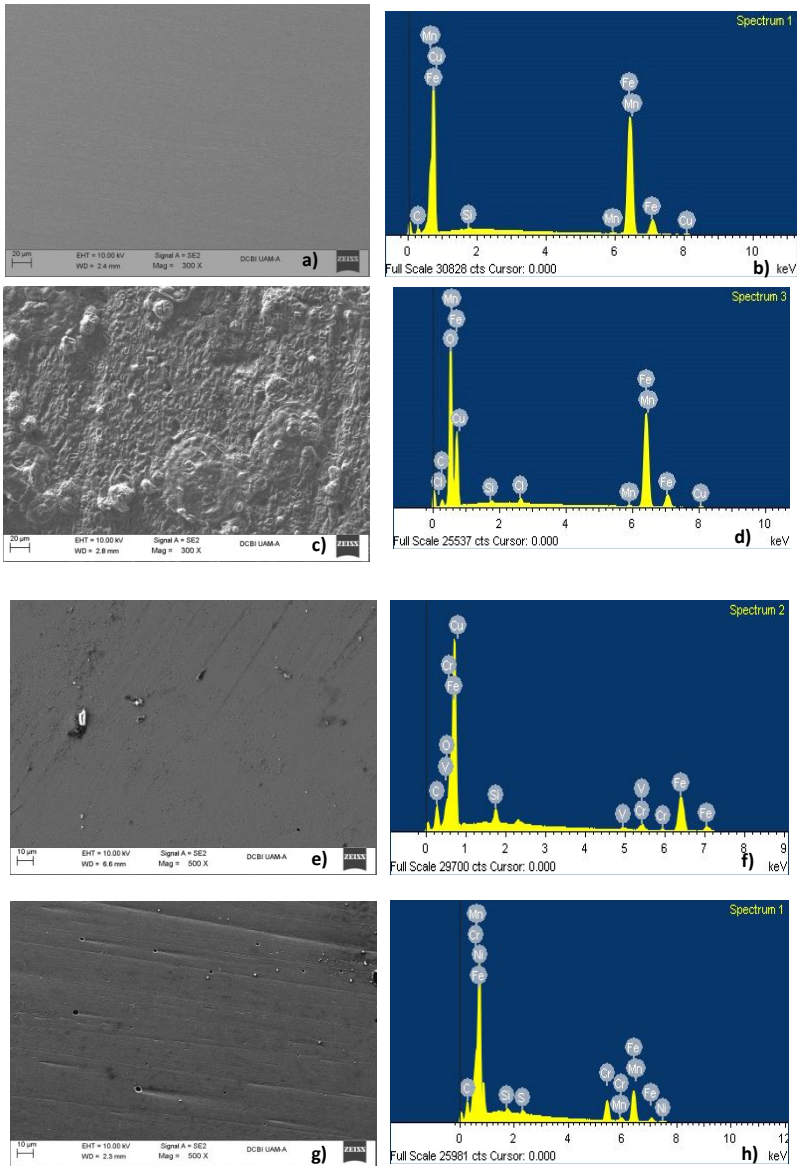
a)
b)
Spectrum 1
Full Scale 30828 cts Cursor: 0.000
keV
c)
d)
Spectrum 3
Full Scale 25537 cts Cursor: 0.000
keV
e)
f)
Spectrum 2
Full Scale 29700 cts Cursor: 0.000
keV
g)
h)
Spectrum 1
Full Scale 25981 cts Cursor: 0.000
keV

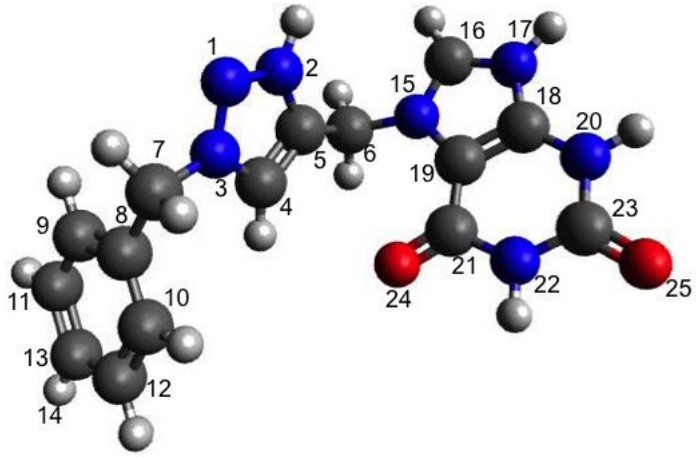

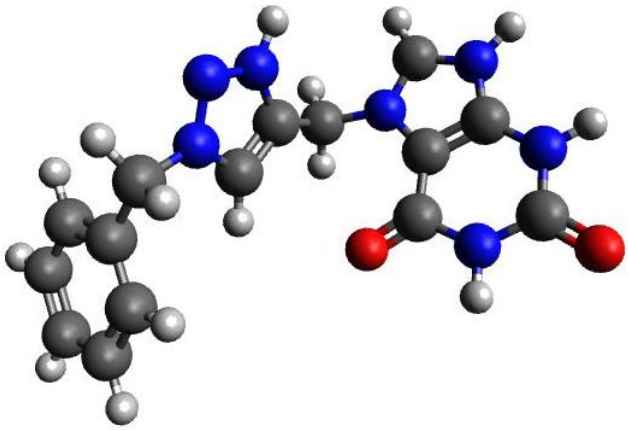

(a) Front.
Dihedral = 100.6°

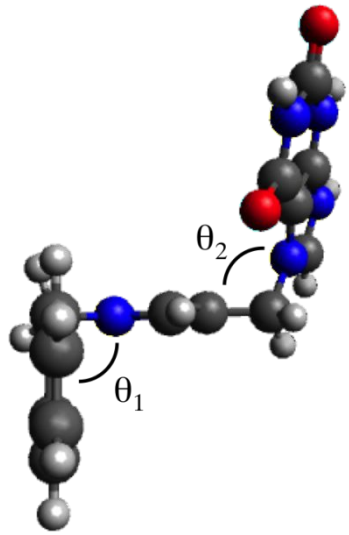

(a) θ_1= 110.9°; θ_2= 111.7°

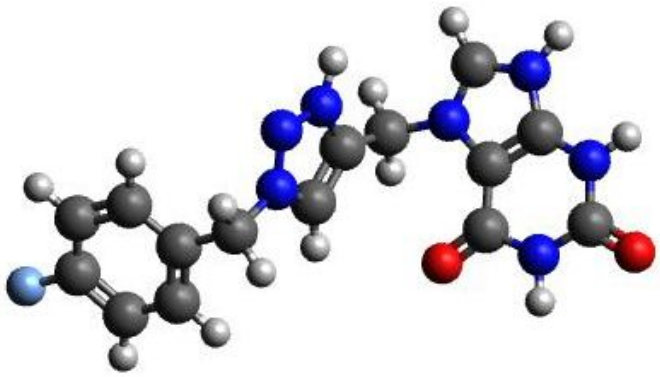

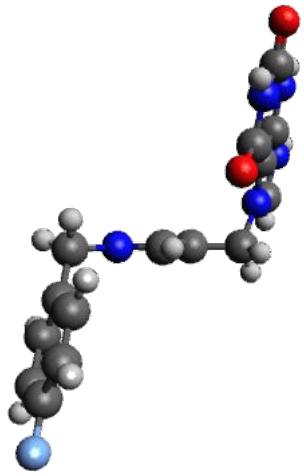

(b) Front, F= blue Dihedral = 97.3°	(b) θ_1= 111.1° ; θ_2= 111.0°
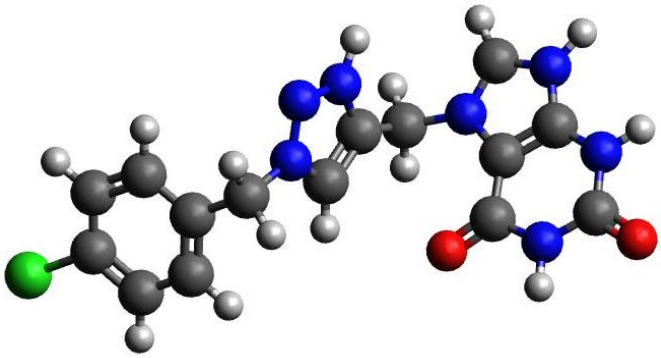	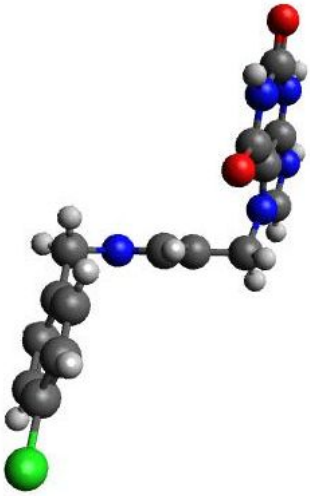
(c) Front, Cl= Green Dihedral = 96.4°	(c) θ_1= 111.1° ; θ_2= 111.2°
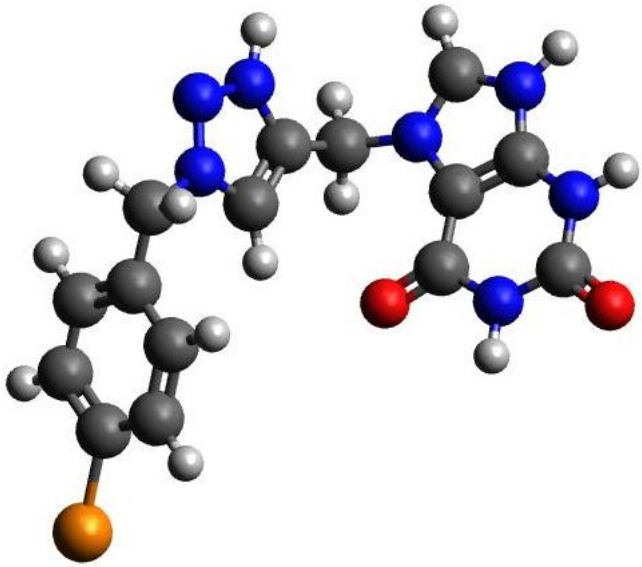	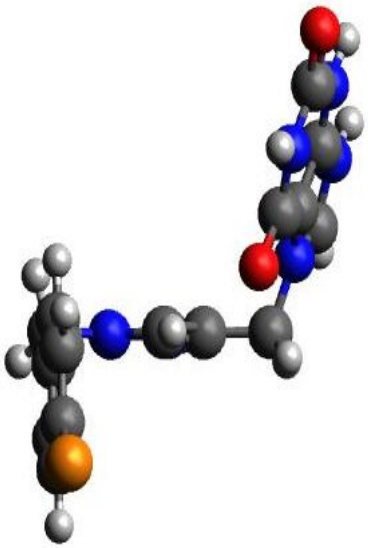
(d) Front, Br= orange Dihedral = 100.9°	(d) θ_1= 110.7°; θ_2= 111.6°

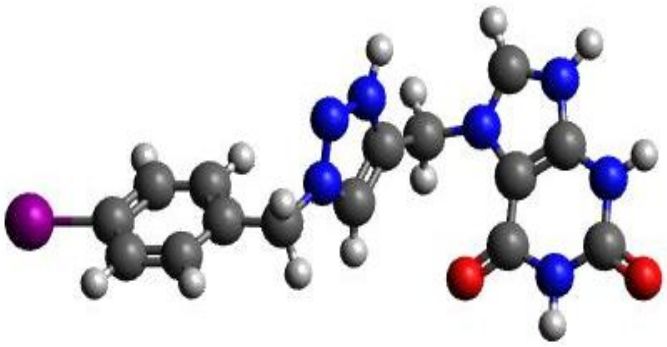	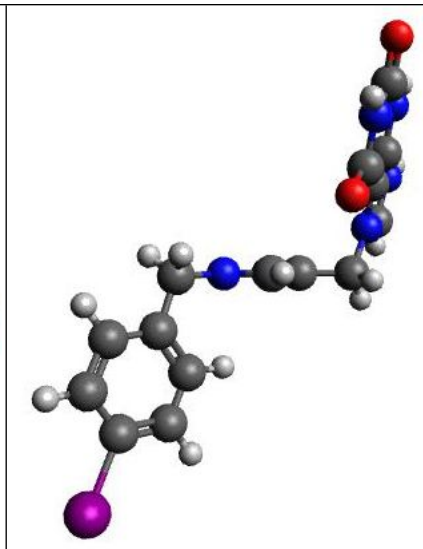
(e) Front, I= purple Dihedral = 1.7°	(e) θ_1= 112.7° ; θ_2= 111.3°